Review Article

Advances in differential diagnosis of cerebrovascular diseases in magnetic resonance imaging: a narrative review

Xin Li[1], Fengbo Su[2], Qinghai Yuan[1], Yan Chen[2], Chun-Yan Liu[1], Yuhang Fan[3]

[1]Department of Radiology, the Second Hospital of Jilin University, Changchun, China; [2]Department of Neurosurgery, the Second Hospital of Jilin University, Changchun, China; [3]Department of Internal Neurology, the Second Hospital of Jilin University, Changchun, China

Contributions: (I) Conception and design: F Su, Q Yuan; (II) Administrative support: Q Yuan; (III) Provision of study materials or patients: F Su; (IV) Collection and assembly of data: X Li; (V) Data analysis and interpretation: All authors; (VI) Manuscript writing: All authors; (VII) Final approval of manuscript: All authors.

Correspondence to: Fengbo Su. Department of Neurosurgery, the Second Hospital of Jilin University, No. 218 Ziqiang St., Changchun 130041, China. Email: sufengbo@jlu.edu.cn; Qinghai Yuan. Department of Radiology, the Second Hospital of Jilin University, No. 218 Ziqiang St., Changchun 130041, China. Email: yqh@jlu.edu.cn.

Background and Objective: Cerebrovascular diseases (CVDs), particularly cerebral stroke, remain a primary cause of disability and death worldwide. Accurate diagnosis of CVDs is essential to guide therapeutic decisions and foresee the prognosis. Different CVDs have different pathological processes while they have many signs in common with some other brain diseases. Thus, differential diagnoses of strokes from other primary and secondary CVDs are especially important and challenging.

Methods: This review is composed mainly based on searching PubMed articles between September, 2013 and December 26, 2022 in English.

Key Content and Findings: Neuroimaging is a powerful tool for CVD diagnosis including cerebral angiography, ultrasound, computed tomography, and positron emission tomography as well as magnetic resonance imaging (MRI). MRI excels other imaging techniques by its features of non-invasive, diverse sequences and high spatiotemporal resolution. It can detect hemodynamic, structural alterations of intracranial arteries and metabolic status of their associated brain regions. In acute stroke, differential diagnosis of ischemic from hemorrhagic stroke and other intracranial vasculopathies is a common application of MRI. By providing information about the pathological characteristics of cerebral diseases exhibiting different degrees of behavioral alterations, cognitive impairment, motor dysfunction and other indications, MRI can differentiate strokes from other primary CVDs involving cerebral small vessels and identify vascular dementia from hyponatremia, brain tumors and other secondary or non-primary CVDs.

Conclusions: Recent advances in MRI technology allow clinical neuroimaging to provide unique reference for differentiating many previously inconclusive CVDs. MRI technology is worthy of full exploration while breaking its limitations in clinical applications should be considered.

Keywords: Cerebrovascular diseases (CVDs); differential diagnosis; magnetic resonance imaging (MRI); neuroimaging; cerebral stroke

Submitted Jul 18, 2022. Accepted for publication Jan 20, 2023. Published online Feb 22, 2023.
doi: 10.21037/qims-22-750
View this article at: https://dx.doi.org/10.21037/qims-22-750

Introduction

Cerebrovascular diseases (CVDs) include any disorders temporarily or permanently disturbing a brain area due to alterations in blood flow and/or blood vessels. CVDs involve pathological alterations in blood vessels of the brain and typically manifest in cerebral stroke. Cerebral stroke is a primary cause of disability and death worldwide and occurs at main branches of the cerebral arteries, basilar arteries, their associated small vessels and corresponding veins (1). Its differential diagnosis can be difficulty, particularly when it involves small vessel and complications with other CVDs (2,3). Moreover, there are many brain diseases not primarily involving cerebral vessels but presenting physical and mental symptoms similar to that of the stroke, such as hyponatremia, multiple sclerosis and brain tumors. Differential diagnosis of strokes from these secondary CVDs is essential to guide therapeutic decisions and predict the prognosis. Alongside clinical presentation and laboratory tests, neuroimaging techniques have become prevailing tools in differential diagnosis of CVDs. Magnetic resonance imaging (MRI), originally named nuclear magnetic resonance, excels other neuroimaging techniques by its features of non-invasive, diverse models/sequences and high spatiotemporal resolution and thus, becomes a powerful tool in differential diagnosis of a variety of CVDs (2,4). Previously, many excellent reviews of neuroimaging have been published. They focus on either general imaging techniques of ischemic CVDs (5,6) or a specific MRI sequence like vessel wall MRI (2,3) and multiparametric quantitative MRI (7). However, a comprehensive overview of MRI sequences and their administration in differentiation of cerebral stroke from other neurological diseases remains to be presented. This review aims to provide neurologists, neurosurgeons and radiologists with an up-to-date overview of MRI knowledge and its administration for differential diagnosis of CVDs. We present the following article in accordance with the Narrative Review reporting checklist (available at https://qims.amegroups.com/article/view/10.21037/qims-22-750/rc).

Methods

Studies including CVDs in MRI published over the last 10 years, including 109/141 (77.3%) published after 2020, were identified via a PubMed search using different combinations of the following search terms: "cerebrovascular diseases", "differential diagnosis", "magnetic resonance imaging", "neuroimaging", "cerebral stroke" and others as presented in *Table 1*. Additional papers were identified by reviewing reference lists of relevant publications. Publications with relative low credibility and non-English publications were excluded. Data were extracted based on their relevance to the topic instead of implementing a systematic approach to paper selection. More details of the method are shown in *Table 2*.

Overview of MRI in diagnosis of CVDs

Neuroimaging techniques include cerebral angiography, ultrasound, computed tomography (CT) scan, and positron emission tomography (PET) as well as MRI and many others. Compared to CT scans, MRIs are more effective at exposing subtle differences between soft tissues, nerves and blood vessels. Using MRI can detect flowing blood and puzzling vascular malformations as well as demyelination disease without beam-hardening artifacts and any ionizing radiation (8,9). Compared to PET, MRI completes one scan faster with a temporal resolution of ~3 seconds (9-11). These advantages make MRI tests the leading neuroimaging techniques in differential diagnosis of CVDs.

Mechanisms underlying MRIs

MRI is a non-ionizing and non-invasive technique based on the phenomenon of nuclear magnetic resonance. It usually uses a high frequency (200 MHz to 2 GHz) of electromagnetic radiation and large magnetic fields of 1–7 tesla (T). MRI applies external magnetic field to line up protons' axes of the tissue under examination and this alignment or magnetization makes atomic nuclei in water aligned with the axis of the MRI scanner, leading to emission of detectable signals after a period of time. Two different relaxation times (i.e., T1 and T2) are commonly applied to characterize tissue magnetization. T1 is the time constant measuring the returning rate of excited protons to equilibrium status longitudinal to the main field. T2 or traverse relaxation time determines the time consumed for removing phase consistency of spinning protons among the nuclei.

Alongside detection of water movement, the MRI also measures other signals. MRI can detect the amount of brain deoxygenated blood that gives off a Blood-Oxygen-Level Dependent (BOLD) signal. The BOLD signal can be transformed into voxels that manifest as a 3 dimensional (3D) image of the brain for tracking neural activity. That is,

increased neural activity can increase blood flow as well as oxygen consumption, which causes increase in deoxygenated blood and emits more BOLD signals. The strength of this technique is having good spatial resolution of 1 mm that is far beyond the resolution of other imaging techniques. Correspondingly, BOLD-based MRI is particularly useful in determining prior mini-strokes (11,12).

Detecting changes in levels of choline, lactate, myo-inositol, N-acetyl aspartate, myelin in tissues is also an important mechanism of MRI. This is achieved by magnetic resonance spectroscopic imaging (MRSI). MRSI is a molecular imaging technique that can noninvasively map metabolite distributions without labeling, and serves as biomarkers for tumor characterization in the brain (13,14). Spectroscopic imaging with MRSI can distinguish vascular from parenchymal disorders and to discern primary from secondary disease manifestations for abnormalities in cerebral blood flow. Fast MRSI of the brain is an alternative approach to shorten scanning time and thus makes MRSI more suitable for clinical application in diagnosis of neurology, multiple sclerosis, stroke and epilepsy (13,15,16). For example, myelin is an important component of the brain tissue and sensitive to multi-exponential T2 relaxation. Thus, it is useful in detecting myelin water imaging. By contrast, iron is present in multiple types of brain cells, particularly in cells involving ferroptosis-associated neurodegeneration. Similar to myelin, iron also decreases T2 signals. Combining T1 and T2 relaxometry for iron and myelin can detect the characterization of tissue alterations, recognize diverse quality in the nature of white matter hyperintensities, and implicate different pathophysiology across brain regions. Applying these techniques revealed that increase in iron deposition in cerebral small vessel disease (cSVD) is related to disability and increased local blood-brain barrier (BBB) permeability (17-19).

The contrast and brightness of cerebral imaging are correlated with the intensity of MRI and can be enhanced by using contrast agents. High-resolution images can be

Table 1 The search terms used

("Cerebrovascular diseases"[Mesh]) AND "Magnetic resonance imaging"[Mesh]
("Magnetic resonance imaging"[Mesh]) AND "cerebral stroke"[Mesh]
("Magnetic resonance imaging"[Mesh]) AND "Sequence"[Mesh]
("Cerebrovascular diseases"[Mesh]) AND "Diagnosis"[Mesh]
("Cerebrovascular diseases"[Mesh]) AND "Differential diagnosis"[Mesh]
("Cerebrovascular diseases"[Mesh]) AND "Neuroimaging"[Mesh]
("Cerebrovascular diseases"[Mesh]) AND "pathogenesis"[Mesh]
("Magnetic resonance imaging"[Mesh]) AND "Neurology"[Mesh]
("Magnetic resonance imaging"[Mesh]) AND "neurological disorders"[Mesh]
("Magnetic resonance imaging"[Mesh]) AND "blood vessels"[Mesh]

Table 2 The search strategy summary

Items	Specification
Date of search (specified to date, month and year)	2022/06/17–2022/12/26
Databases and other sources searched	PubMed
Search terms used (including MeSH and free text search terms and filters)	See *Table 1* for details
Timeframe	2013–2023
Inclusion and exclusion criteria (study type, language restrictions, etc.)	Inclusion criteria: research articles and reviews in English about themes such as *cerebrovascular diseases and magnetic resonance* imaging. Exclusion criteria: some papers with low reliability we considered or non-English
Selection process (who conducted the selection, whether it was conducted independently, how consensus was obtained, etc.)	Xin Li conducted the selection, all authors attended a meeting to discuss the literature selection and obtained the consensus
Any additional considerations, if applicable	Some papers were identified by reviewing reference lists of relevant publications. Among papers with similar content, priority of citation was given to newly published work

obtained by applying 1.5T and 7T MRIs. For instance, 7T MRI provides enhanced details in cortical imaging ≤1 millimeter of tissue, and reduces blurring between gray and white matter. Thus, 7T MRI can display detailed characteristics of the small vessels that are invisible in a conventional 3T MRI. Using 7T MRI can detect early pathological alterations in small vessels and thus guide evaluation of treatment effects on vascular functions at early stage (17,20,21). Moreover, by administration of a gadolinium-based contrast agent, dynamic contrast-enhanced (DCE)-MRI can detect permeability and fluid volume fractions of blood vessels in cSVD, which overcomes the limitation of conventional MRI that is difficult to detect increase in BBB permeability (21,22).

Sequences and applications of MRIs in diagnosis of CVDs

MRIs are a continuously developing technology that evolves upon the challenges of clinical demands for high resolution and fast reports of the test. MRIs can be used in many different models/sequences and in combination with other imaging techniques.

Basic sequences of MRIs

In MRI sequences, T1-weighted and T2-weighted scans are the most commonly used. T1-weighted images (*Figure 1A*) can highlight fat tissue within the body by use of short "time to echo" alongside "repetition time". T1 properties of tissues are the dominant factor determining the contrast and brightness of an image. By contrast, T2-weighted image (*Figure 1B*) can highlight fat and water within the body by use of longer time to echo and repetition time. These features allow MRI test to identify atherosclerosis and hemodynamic alterations. In addition, proton-density changes and subsequent signal enhancement by water protons in extravascular space can reflect cellular swelling in prefrontal cortex and other tissues interfacing air and/or bone or close to large blood vessels (23,30).

Diffusion-weighted imaging (DWI)

DWI measures water molecule diffusion in tissues (*Figure 1C*). As diffusing water interacts with many different obstacles throughout biological tissues, DWI can demonstrate the details of tissue architecture and quantify changes in hemodynamic. For fibrous internal structures like axons in white matter, early tissue alterations that are not detectable in conventional imaging can be quickly captured by diffusion tensor imaging. In these tissues, water diffuses faster along the axons or blood vessels than in the direction perpendicular to it. This feature is helpful in determining fractional anisotropy that has different value when measured in different direction, connectivity and other characteristics of the tissue. Thus, DWI can help reconstruct structural brain networks that excels functional network analysis for cSVD at resting condition (24,31,32).

In association with DWI, apparent diffusion coefficient (ADC) measures the average size and size distribution of alveoli and acinar airspaces and can quantify restriction of water diffusion. Calculating DWI/ADC ratio can provide optimized information about cell count, proliferation markers and other histological architecture of tissues (33,34).

Susceptibility-weighted imaging (SWI)

SWI, originally named BOLD venographic imaging, is developing from simple 2D to 3D T2-weighted sequences having better spatial resolution and contrast of susceptibility (*Figure 1D*). It is particularly sensitive to compounds with paramagnetic, diamagnetic, and ferromagnetic properties, which can identify deoxyhemoglobin, ferritin, hemosiderin, calcium and some other blood products. SWI has the advantage of phase and magnitude and can reveal small amounts of hemorrhage or calcium. It is also used for assessing veins as deoxyhemoglobin causes losing magnitude and shifting the phase (35).

DCE-MRI

DCE-MRI can measure perfusion, fluid volume fractions, vessel permeability, and other microvascular parameters quantitatively. DCE-MRI can measure small changes in BBB permeability in serial T1-weighted scanning through ~25 min after using a gadolinium-based contrast agent. Through measuring the delivery rate of contrast agent to the extravascular space and its levels, DCE-MRI can demonstrate increases in BBB permeability in cSVD (*Figure 1E*). In addition, DCE-MRI test is very useful in prognosis and individualized management of CVDs, such as cSVD-related stroke, vascular cognitive impairment and diseases involving white matter that all change BBB permeability (21,22).

Cerebrovascular reactivity (CVR)

This MRI measurement probes cerebral hemodynamic changes following vasodilatory stimulus. Using carbon dioxide inhalation and BOLD, CVR mapping has high sensitivity and spatial resolution through simple processing, and thus can provide a better approach to detect CVDs. CVR can measure the initial BBB leakage and subsequent stiffness, which is a key to understanding the pathogenesis of stroke, cSVD and dementias. Baseline CVR may predict progress of subsequent cSVD, drug response and individualize medications. Lower CVR is related to cognitive impairment that is caused by worsened white

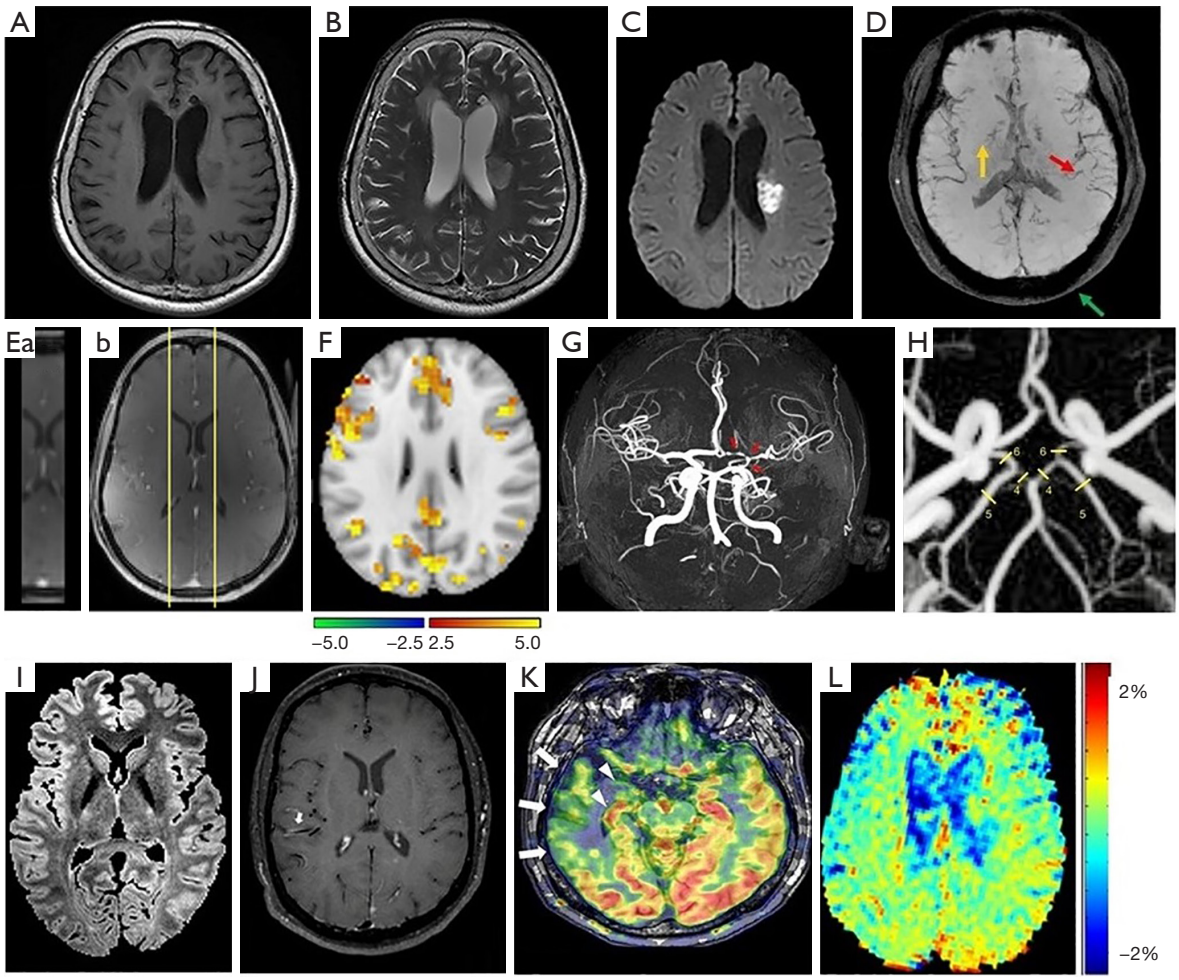

Figure 1 Basic MRI sequences. (A) T1-weighted-weighted scans. (B) T2-weighted scans. (C) DWI. (A-C). MRI from patient with acute ischemic stroke [reprinted with permission from Lin *et al.* (23)]. (D) SWI. Some small vessels are marked in red arrows, the red nucleus is marked in yellow arrows, the skull and extracranial lipid are marked in green arrows [reprinted with permission from Qiu *et al.* (24)]. (E) DCE-MRI. Images of the fast (during contrast) DCE-MRI part at the highest contrast agent concentration (a), and first dynamic phase of the slow (postcontrast) DCE-MRI part after contrast agent arrival (b). The smaller brain area (yellow border lines), planned through the superior sagittal sinus, is acquired for the fast (during contrast) part to obtain shorter dynamic scan intervals [reprinted with permission from de Canjels *et al.* (21)]. (F) CVR. Brain regions showing significant effects of clinical composite score 1 on the BOLD signal change from the acute to subacute phase of injury [reprinted with permission from Churchill *et al.* (25)]. The scales are bootstrap ratio. (G) MRA. Time of flight-MRA showing stenotic lesions in the terminal part of internal left carotid, middle and anterior left cerebral arteries (red arrows) in a patient presenting with a secondary central nervous system angiitis in the context of systemic lupus erythematosus [reprinted with permission from Ferlini *et al.* (26)]. (H) 4D flow MRI. Blood flow is measured in P1 and P2 segments of the posterior cerebral artery [4, 5], and the posterior communicating arteries [6] [reprinted with permission from Malm *et al.* (27)]. (I) T2/FLAIR. In an axial F section, lower intensity values with a greater degree of myelination [reprinted with permission from Ganzetti *et al.* (28)]. (J) IVW-MRI. Image shows multiple areas of concentric contrast enhancement in the proximal left and distal right of the middle cerebral arteries (arrows) in a patient presenting with primary angiitis of the central nervous system [reprinted with permission from Ferlini *et al.* (26)]. (K) ASL-MRI. Interictal ASL shows ipsilateral hypoperfusion in the temporal neocortex (arrows) and in the medial temporal lobe (arrowhead) [reprinted with permission from Sone *et al.* (29)]. (L) APTw-MRI. Image is from a patient with acute ischemic stroke [reprinted with permission from Lin *et al.* (23)]. MRI, magnetic resonance imaging; DWI, diffusion-weighted imaging; SWI, susceptibility-weighted imaging; DCE, dynamic contrast-enhanced; CVR, cerebrovascular reactivity; BOLD, blood-oxygen-level dependent; MRA, magnetic resonance angiogram; 4D flow MRI, four-dimensional flow magnetic resonance imaging; FLAIR, fluid-attenuated inversion recovery; IVW, intracranial vessel wall; ASL, arterial spin labeling; APTw, amide-proton-transfer weighted.

matter hyperintensity, as shown in patients of minor stroke (*Figure 1F*). Assessment of CVR with BOLD MRI can yield excellent spatial resolution while having fine repeatability, reproducibility and tolerability. By administering higher field strength to increase BOLD signals, CVR imaging may yield larger and more weighted images for cSVD (25,36,37).

Magnetic resonance angiogram (MRA)

MRA can evaluate blood flow of the carotid arteries, vertebral arteries, basilar artery and branches of these vessels as well as venous sinuses in CVDs. MRA is usually performed on patients whose head and neck surgery are expected. MRA can specifically examine blood vessels and help discover blockage and aneurysms (17). Time-of-flight MRA (*Figure 1G*) is the dominant non-contrast bright-blood method in grading residual aneurysm, and has been introduced for imaging human vascular system, and differential subsampling with an ultrafast high-spatial-resolution head MRA (26,38,39).

Four-dimensional flow MRI (4D flow MRI)

It is a multi-modality approach using phase-contrast MRI to enhance assessments of blood flow and hemodynamic analysis in cerebral aneurysms and other CVDs. It uses a collection of high-resolution velocity fields to reconstruct the flow field (*Figure 1H*), which increases the spatial resolution and velocity accuracy in synthesizing MRI data, and thus provides reliable evaluation of pressure and wall shear stress in cerebral aneurisms while providing volumetric and time-resolved visualization and quantification of blood flow (27,40-42).

T2/Fluid-attenuated inversion recovery (FLAIR)

FLAIR is an inversion recovery set of MRI sequence that suppresses the intensity of fluids like cerebrospinal fluid (CSF) but highlights areas of tissue T2 prolongation, and exposes lesions adjacent to CSF clearly, such as cerebral cortical regions. Thus, FLAIR can avoid influences of CSF on detection of the periventricular hyperintense lesions (*Figure 1I*). In an axial F section, lower intensity values with a greater degree of myelination in the FLAIR technique (28). In T1 C+ image, peri-tumoral edema appears in ring enhancement hyperintense pattern in FLAIR image (15,16).

Intracranial vessel wall (IVW)-MRI

IVW-MRI can detect MRI signal of the thinner artery wall (relative to luminal diameter) and its thickening in vessel wall disease while suppressing the MRI signal arising from neighboring blood and CSF within the voxel. IVW-MRI has an overall sensitivity closing to that of digital subtraction angiography for vasculitis diagnosis. IVW is helpful in differentiation of vasculitis from intracranial atherosclerotic disease, intracranial arterial dissection or reversible vasoconstriction syndrome. Vasculitis in IVW is characterized by a multifocal or diffuse homogenous concentric enhancement of the vessel wall (*Figure 1J*). In detecting angiitis of the central nervous system, IVW has a 95% specificity and 94% sensitivity for the diagnosis (26).

Arterial spin labeling (ASL)-MRI

ASL-MRI can noninvasively measure cerebral blood flow by labeling inflowing blood magnetically. It can be used to detect hypoperfusion in dementia, assess perfusion alterations in stroke, identify blood shunting in arteriovenous malformations and dural arteriovenous fistulas, localize epileptogenic focus in epilepsy, and differentiate malignant from benign tumors (29). For example, interictal ASL detects ipsilateral hypoperfusion in the temporal neocortex in temporal lobe epilepsy (*Figure 1K*).

Amide-proton-transfer weighted (APTw) MRI

APTw-MRI belongs to chemical exchange saturation transfer imaging. It uses the mechanism of frequent exchange between amide protons of small molecules and the surrounding water protons as well as the transfer of nuclear spin saturation from amide protons to water protons, which reduces water proton signal. APTw values can reflect cell proliferation and serve as biomarkers of tumor malignancy while characterizing CVDs (23), such as ischemic stroke (*Figure 1L*).

Other MRI sequences

In addition to those that are listed above, other sequences and measurements have also been developed. Optical coherence tomography (43), ultrafast high spatial-resolution MRA (44) and other emerging techniques (45,46) also offer similar insights into CVDs. In clinical scenarios, different imaging techniques are often used together to gain mechanistic insights for a series of cerebrovascular pathologies.

Stroke and its diagnosis with MRI

CVDs mainly embrace stroke, carotid stenosis, vertebral artery stenosis, intracranial stenosis, aneurysms, and vascular malformations. Primary CVDs can change brain functions and cognition while many non-primary CVDs can influence the structure and functions of cerebral vessels as well. Rapidly and accurately differential diagnosis of these diseases using MRI is the key to managing these diseases efficiently (5,47,48).

Ischemic cerebral stroke

Stroke refers to the circulation status of lacking sufficient blood flow to irrigate brain tissue due to either intra-vessel blockage, vessel narrowing or hemorrhage. More than 80% of strokes are ischemic and the rest are hemorrhagic (49,50).

General clinical features

The leading cause of ischemic stroke is atherosclerosis and then hypertension. Ischemic stroke can manifest as changes in levels of consciousness, and many functions of motor and sensation. With a clear history and careful physical exam, a stroke and its cerebral location can be identified. Although occlusion at different segments of the cerebral vessels can exhibit different symptoms and signs, the infarct areas present basically the same pathologic alterations (51,52), which form the basis of neuroimaging diagnosis of ischemic stroke (*Figure 1C*, *Figure 2A*).

In ischemic stroke, lacunar stroke occupies about 20% and results from occlusion of small penetrating branches of cerebral vessels (*Figure 2B*). In this cSVD, occlusion of individual lenticulostriate arteries leads to lacunar stroke and cognitive impairment, which can be pure motor, pure sensory or ataxic hemiparetic strokes. In addition, at the early stage, signs of motor disturbance may not be obvious, and timely differential diagnosis with MRI becomes important (56,57).

Diagnosis of stroke

In general, clinical presentation is the main diagnosis of stroke. However, the diagnosis at the very early stage of stroke can be difficult, especially when stroke is complicated with brain lesions showing ischemic stroke-like injuries. Thus, MRI characterization of ischemic neuroimaging is essential for diagnosis of stroke (53,54).

DWI can detect ischemic lesions accurately (*Figure 2A*, *2B*). In general, the lesions manifest as hyperintense areas on DWI and as correlative hypointense regions on ADC maps, which appear as quick as minutes of stroke onset. Notably, MRI can detect small lesions in cortical or subcortical areas, more effortlessly than CT scan at the acute stage, especially in the posterior fossa or brain stem (58-61).

At different stages of stroke, different manifestations of neuroimaging are present. Arterial occlusion enhances DWI signal and reduces ADC values in the infarct core within minutes. Changes in blood flow appear in MRA and thromboembolism can be identified with SWI. Slow or stagnant flow due to loss of normal flow void in vessels may also be detected as high signal on FLAIR (*Figure 2A*) and T1 C+ intravascular enhancement. From 6 hours of stroke onset, high T2 signal can be increasingly revealed on FLAIR. After 16 hours of stroke, T1 hypointensity appears. During the first week, high DWI signal and low ADC signal persist in the infarct parenchyma while the infarct area still appears hyperintense on T2 and FLAIR. Cortical contrast enhancement usually lasts for 2–4 months (62,63). In animal study, capillary thrombosis following the venous thrombosis can be found. In rats of sexes, T2 lesion volume and neurological function is correlated with the number of T2*-positive thrombotic vessels, which is significantly greater in female than male rats (64).

Studying blood flow velocity of small perforating arteries is critical to capture earlier pathological alterations in lacunar stroke with 7T phase contrast MRI. Velocity pulsatility can be measured from these blood flow velocity. Arterial pulse pressure may be partially dampened by stiff vessels, which causes arterial transmission of higher pulsatility. Assessing pulsatility with CVR in these small vessels helps reveal the pathways underpinning cSVD (65,66). These changes are also exhibited in *Figure 2A*.

Hemorrhagic stroke

General clinical features

A hemorrhagic stroke is bleeding directly into the brain tissue caused by traumatic injury, hypertension, amyloid angiopathy, hemorrhagic conversion of ischemic stroke, cerebral aneurysms, arteriovenous malformations and vasculitis alongside other causes like dural arteriovenous fistula and venous sinus thrombosis (67). Acute hemorrhagic stroke includes subarachnoid hemorrhage (SAH), subdural hematoma or intraparenchymal cerebral hemorrhage. The symptoms include headache, one-sided weakness, decreased level of consciousness, neck stiffness, increased intracranial pressure, vomiting, seizures and others (68,69).

Diagnosis of hemorrhagic stroke

Neuroimaging is essential for identification of the cause, location, severity, guidance of treatment, prognosis of cerebral injury of hemorrhage. The age of the hematoma is important sign for MRI evaluation of intracranial hemorrhage (*Figure 2C*).

In general, hemorrhagic stroke in axial MRI appears as a hyperacute hematoma in the brain that is isointense to hypointense in axial T1-weighted image and hyperintense on T2-weighted imaging. It often manifests as low signal intensity with a small rim of vasogenic edema surrounding the hematoma. A conventional intermediate-echo T2-weighted 3.0-T image can detect hemosiderin and bleeding while SWI can further reveal diffuse microbleeds (*Figure 2C*) and vascular damage and highlight the veins based on their high levels of deoxyhemoglobin content (67). At 1 month,

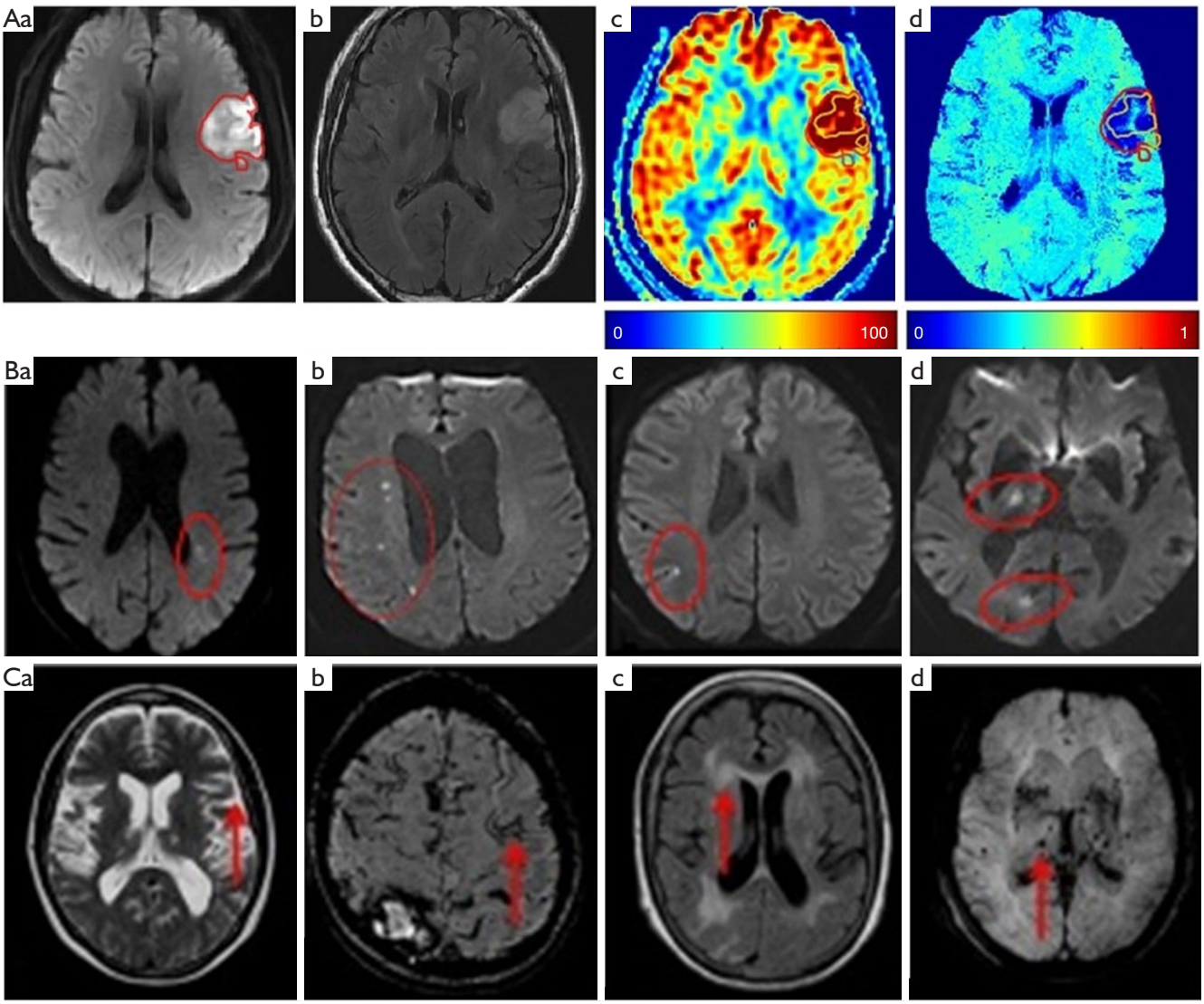

Figure 2 MRI illustration of cerebral stroke. (A) Ischemic stroke. Representative images showing the infarct at 58-h in DWI (a, red circle), T2/FLAIR (b), cerebral blood flow (c) and oxygen extraction fraction (d). Reprinted with permission from Wu *et al.* (53). (B) Lacunar stroke. Stroke topography on DWI in single subcortical (a), multiple subcortical (b), cortical (c), and non-confluent cortical-subcortical regions (d). Reprinted with permission from Tan *et al.* (54). (C) Hemorrhagic stroke. T2 weighted axial MRI of the brain showing severe cerebral atrophy (a, red arrow); axial MRI of the brain demonstrating a linear gyriform hypointensity (b, red arrow) on SWI sequence in a cortical distribution representative of superficial siderosis; T2/FLAIR weighted MRI showing large confluent lesions (c, red arrow) with a Fazekas 3 rating and maximum intensity projection of SWI sequence of the brain showing multiple diffuse microbleeds (d, red arrow). Reprinted with permission from Karayiannis *et al.* (55). MRI, magnetic resonance imaging; FLAIR, fluid-attenuated inversion recovery; DWI, diffusion-weighted imaging; SWI, susceptibility-weighted imaging.

the susceptibilities, fractional anisotropy, and cerebral blood flow decrease in the perihematomal tissues relative to the contralateral side, whereas mean diffusivity enhances. In the hematomal tissues, the susceptibilities increase; however, fractional anisotropy, mean diffusivity and cerebral blood flow decrease relative to the contralesional area. At 3 months, hematoma and perihematomal volumes reduce significantly (70).

In the differential diagnosis, if the patient has severe sharp headache, SAH should be considered. Within 48 hours of

traumatic brain injury, relative to non-SAH patients, lower perfusion in the acute phase of SAH indicates higher risk for brain volume loss (71,72). Consistently, in rat SAH model with endovascular perforation or sham surgery, T2 and T2* MRI tests at 24 h after SAH onset exhibit increase in the numbers of T2* hypointense vessels. The increased vessel number correlates to SAH severity in MRI-based grading of bleeding (64).

In addition, MRI can localize the hemorrhage while providing information about local oxygen partial pressure in the tissues, patient's hematocrit, local glucose concentration, the regional acidity, hemoglobin concentration, and integrity of the BBB. Lastly, SWI excels CT scan in differentiation of hemorrhagic transformation of ischemic infarction, hemorrhagic venous infarct, cerebral venous sinus thrombosis, and hypertensive microhemorrhage as well as cerebral amyloid angiopathy (55,73).

Differential diagnoses of stroke from other CVDs with MRI

While atherosclerosis is the predominant cause of various strokes, transient ischemic attack (TIA), cerebral aneurysm, vascular malformations, carotid stenosis and moyamoya disease can also change cerebral hemodynamic and even evoke stroke-like disorders in brain functions and cognition. Thus, these CVDs need to be differentiated from atherosclerotic stroke.

TIA

General clinical features

When a cerebral artery is blocked temporarily, TIA occurs. TIA may exhibit stroke-like symptoms; however, this temporary event does not cause permanent damage. TIA often results from transient blockage of cerebral blood vessel by an embolus or thrombus and their subsequent dissolve allows blood flow to resume without permanent damages. Vasospasm is another etiology leading to temporary narrowing of the blood vessel lumen. The patients may develop into strokes, especially shortly after a TIA attack. To prevent strokes in patients with TIA, urgent evaluation and intervention should be performed (74,75).

Diagnosis of TIA

The occurrence of TIA is generally too short to be detected in MRI (*Figure 3A*). However, MRI may show evidence of an infarct or hemorrhage to rule out a TIA or to identify the reason of TIA, such as carotid plaques (80). In inpatients, MRI is the most sensitive imaging method of detecting TIA or minor stroke; acute DWI hyperintense lesions on brain MRI can match 29.3% patients with a clinical diagnosis of TIA (74). However, the hyperintensity on DWI decreases after 10 days and totally disappears at 2–3 weeks after the original attack. Thus, it is recommended to complete diagnosis of TIA in DWI within 24 hours of symptom onset since TIA differs from stroke in the symptoms that usually last less than an hour without permanent brain damage in MRI (76,81,82).

Cerebral aneurysm

General clinical features

When an area of artery wall in the brain weakens, part of the vessel wall expands to form cerebral aneurysm. Cerebral aneurysm can result from aging, high blood pressure, atherosclerosis, head trauma or other conditions that weaken vessel walls. Unruptured intracranial aneurysms exist in 1–5% of the general population. Only 0.25–0.5% percentage of aneurisms rupture and form SAH. Patients with unruptured intracranial aneurysms usually appear mild to severe headaches, vision impairment and many other symptoms depending on the site and size of the aneurisms (83,84).

Diagnosis of cerebral aneurysm

MRI can produce detailed images of cerebral aneurysms in phase-contrast sequence that can enhance blood flow measurements and hemodynamic analysis in patients (85). After endovascular treatment, DCE-MRA through differential subsampling with Cartesian ordering-MRA has higher accuracy and time-efficiency in detection of cerebral aneurisms with ultrafast process and high-spatial-resolution. It shows dramatic changes in inflow hemodynamic, inflow jet patterns, and vortex; the highest velocity differences are present at tissues close to the wall and vessel bifurcation along with change in parent vessel pulsatility (44,75,86,87). *Figure 3B* shows neuroimaging of an aneurysm of the basilar artery in several sequences of MRI relative to that in CT.

Vascular malformations

General clinical features

Vascular malformation is due to abnormal connection of an artery, vein or both of them. It often manifests as arteriovenous malformation, dural arteriovenous fistula, cavernous malformation or hemangioma and venous malformation. The malformation is usually congenital and has abnormal blood flow in the brain. The main symptoms of the vascular malformations include headaches, seizures, strokes, or hemorrhage (88-90).

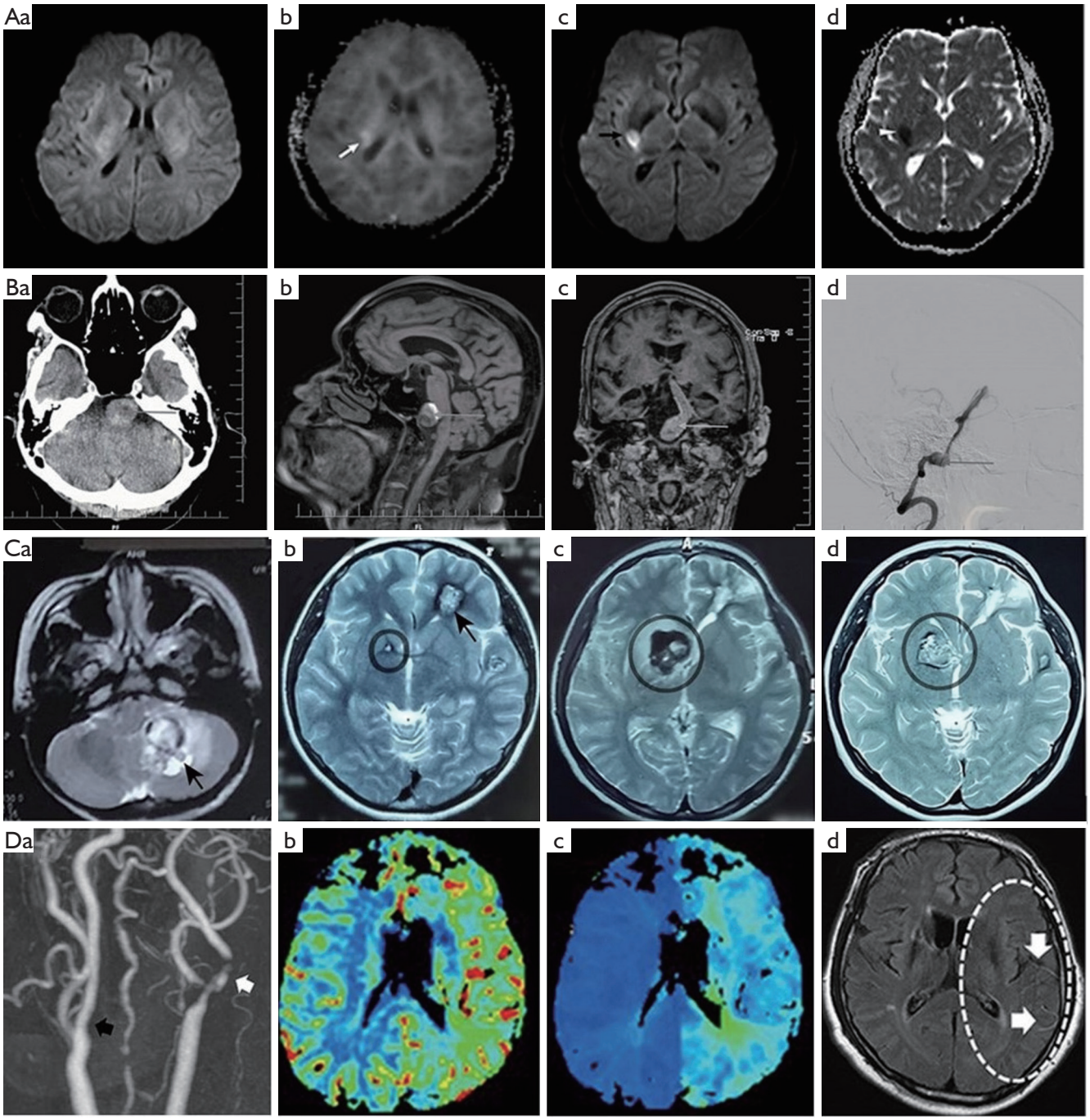

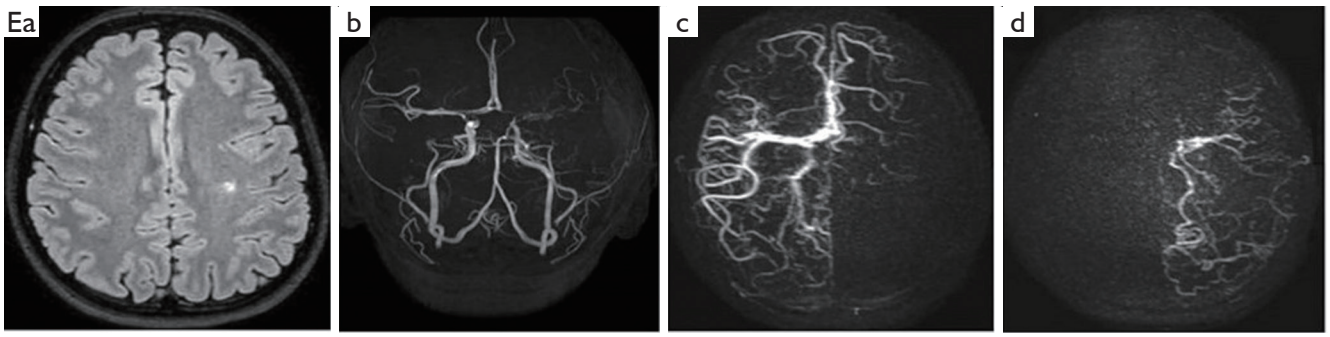

Figure 3 MRI illustration of CVDs other than stroke. (A) TIA: images showing no abnormality on the initial DWI scan (a), a hyperintense area in the right basal ganglia on the baseline mean kurtosis map (b, white arrow) and a new ischemic lesion is present in a similar location in the right middle cerebral artery territory on follow-up DWI (c, black arrow) and apparent diffusion coefficient maps (d, white arrowhead) 10 days later, respectively [reprinted with permission from Zhou *et al.* (76)]. (B) Aneurysm: CT brain axial section showing a dilated basilar artery, suggestive of an aneurysm, compressing the left pons (a, arrow); MRI brain sagittal section showing a partially thrombosed basilar artery aneurysm (b, arrow); MRI brain coronal section showing a dilated basilar artery, and basilar artery aneurysm (c, arrow) and cerebral angiogram confirming a fusosaccular aneurysm arising from V3, V4 segments of left vertebral artery and basilar artery (d, arrow) [reprinted with permission from Bhat *et al.* (75)]. (C) Malformations. MRI (T1-weighted) detects a lesion located in the left cerebellar hemisphere (a, black arrow) when the patient with cerebral cavernous malformations has the first hemorrhage. At the second hemorrhage, MRI (T2 weighted) shows a lesion in the left frontal lobe (b, which is surgically removed) and a small lesion in right basal ganglia (c and d, black circle) [reprinted with permission from Zhang *et al.* (77)]. (D) Carotid stenosis. MRA shows stenosis of the proximal internal carotid artery (a, white arrow) and contralateral carotid artery stenosis (a, black arrow). In perfusion-weighted imaging, increased cerebral blood volume (b) and delayed time to peak (c) are shown. FLAIR shows hyperintense vessel signal in FLAIR (d, white arrows) [reprinted with permission from Park *et al.* (78)]. (E) Moyamoya disease. FLAIR reveals a subacute postischemic lesion in the left-hemispheric white matter (a) and time-of-flight magnetic resonance angiography shows multiple changes of arterial vascular calibers (b). Super-selective 4D ASL-based MRA and digital subtraction angiography of the right-sided ICA (c) and left-sided ICA (d) shows aberrant interhemispheric supply patterns in time-resolved manner [reprinted with permission from Sollmann *et al.* (79)]. TIA, transient ischemic attack; CVDs, cerebrovascular diseases; DWI, diffusion-weighted imaging; MRI, magnetic resonance imaging; MRA, magnetic resonance angiogram; FLAIR, fluid-attenuated inversion recovery; ASL, arterial spin labeling; ICA, internal carotid artery.

Diagnosis of vascular malformations

The wide range of pathological conditions of vascular malformations makes some present typical neuroimaging features (*Figure 3C*) and others appear untypical. The MRI diagnosis of vascular malformations involves spin echo or fast spin echo T1-weighted imaging for regional anatomy, and spin echo T2-weighted imaging for delineating the degrees of the abnormality. Spin echo T2-weighted imaging can differentiate areas of bleeding from high-flow or hemosiderin deposition. DCE-MRI can quickly acquire image with high specificity for differentiating venous malformation from non-venous malformations, which yields a volumetric dataset of high spatial and temporal resolution. Time-resolved angiography techniques can differentiate high-flow from low-flow lesions based on their hemodynamic based on its assessments of flow direction, feeder arteries and drainage veins (77,89,91,92).

Carotid stenosis

General clinical features

Atherosclerosis or other etiologies occurring at the carotid arteries can cause reduction in the diameter of the internal carotid arteries and even blockage, forming carotid stenosis. Carotid stenosis often results in TIA or stroke when pieces of plaque get into the brain, and subsequently temporal or permanent signs of cerebral ischemia. Carotid stenosis should be differentiated from carotid web and carotid dissection in diagnosis (93-95).

Diagnosis of carotid stenosis

MRI can identify stenotic carotid arteries, and characterize the size, composition, and activity of atherosclerotic plaque (*Figure 3D*). In patients with carotid stenosis, using gradient-echo MRI can detect the absence of plaque calcification, deep white matter hyperintensity and susceptibility vessel sign while using perfusion-

weighted MRI can show increase in cerebral blood volume (96,97). Patients with severe carotid stenosis can exhibit multiple hypointense vessels in the cerebral hemisphere ipsilateral to vessel occlusion/stenosis in SWI. In addition, changes in blood flow are correlated with the extent of carotid stenosis (4,78,98).

Moyamoya disease

General clinical features

Moyamoya disease usually results from progressive disorders in the carotid arteries and their major branches that cause irreversible blockage of cerebral vessels. Children with this disease can accompany with many other complications including strokes, TIA, slowly progressive cognitive decline, seizures or involuntary movements of the extremities. Adult patients without surgery treatment often have intracranial hemorrhages that can change the cerebral structure and organization of the structural covariance network (99-101).

Diagnosis of moyamoya disease

Using structural MRI and graph theory in moyamoya disease can demonstrate the structural covariance network (*Figure 3E*). Moyamoya disease can change both overall and local properties of this network with and without major stroke or hemorrhagic damage. Patients often show a suboptimal structural covariance network with decreased integrity and pronounced volume loss, and regional nodal betweenness centrality (a measure of central situation in a graph based on shortest paths) of the bilateral medial orbitofrontal cortices is significantly decreased (79,98,102,103).

Other brain diseases mimicking CVDs

Many brain diseases do not involve cerebral vessels initially; however, their development can cause disorders in brain functions, disturbance in hemodynamic and even disruption of vessels structures, thereby exhibiting stroke-like symptoms. Alongside clinical manifestations and other neuroimaging tests, MRI tests are critical tool in differentiating vascular from parenchymal abnormalities as well as the management of post-disease rehabilitation.

Functional neurological disorders

Some diseases do not have significant structural changes in brain but show neurological disorders. These diseases include hypoglycemic encephalopathy, hyponatremia, syncope, conversion disorder and hemiplegic migraine, at least.

Hypoglycemic encephalopathy

This brain injury is caused by prolonged or severe hypoglycemia. On both T2 and FLAIR, it manifests as bilaterally increased signals at the posterior limb of the internal capsule, and impaired parieto-occipital cortex, insula, hippocampus and basal ganglia. Diffusion is restricted at early stage and the changes are commonly reversible (38,104-106).

Hyponatremia

Hyponatremia refers to the condition that sodium levels are less than 135 mili-equivalents per liter. Severe hyponatremia occurs when sodium levels down to <120 mili-equivalents per liter in ~30% of patients in intensive care units. In MRI scan at 1.5T at initial presentation of day 1, there is no signal abnormality in the brain parenchyma. Similarly, there are no detectable acute infarct, intracranial hemorrhage, or any focal lesion in DWI with ADC maps, T1-weighted and T2-weighted fast spin-echo images, and FLAIR sequences. In the occurrence of demyelination due to inappropriate correction of hyponatremia, reduced myelin signal in medulla white matter may be identified (38,104-106).

Syncope

When blood flow to the brain drops at low blood pressure, syncope occurs and appears abrupt and transient loss of consciousness. The patient usually has no any illnesses or symptoms after recovery from syncope, such as headache, cognitive deficits, or somnolence. DCE-MRI may detect BBB disruption following syncope and show bright blue colored lines within the sulci throughout the cerebral cortex in severe case (107,108).

Conversion disorder

Patients exhibit motor and sensory symptoms that are unrelated to brain structural lesions although that may sustain this functional neurological disorder. In conversion disorder, microstructural changes in sensory-motor integration occur in both the hand and foot regions (109). Functional MRI of the brain in people with conversion disorder can detect reduced volumes of right and left basal ganglia and right thalamus (110). Moreover, aberrant functional connectivity of limbic-motor regions has been identified in MRI, which exhibits bottom-up hyperactive neural activity in limbic regions and a potential failure of top-down regulation from prefrontal regions (111).

Hemiplegic migraine

Migraine affects 15–20% of people and hemiplegic migraine makes up <1% of these cases. This rare variety of migraine with aura can exhibit many visual symptoms, like flashes of light and zigzag patterns, which happen before or during

a migraine episode. Loss-of-function mutations of the gene of alpha 1A subunit of P/Q type voltage-dependent calcium channel can account for this disease. In MRI, patients of hemiplegic migraine can exhibit a mild atrophic cerebellum and many hyperintense lesions of the cerebral white matter without symptoms. However, the remarkable MRI presentation lacks specificity while other examinations appear normal (112-114).

Structural neurological disorders or lesions

Structural neurological disorders represent structural changes; however, the involvements in cerebral vessels or their functions are minor or secondary. These disorders include hydrocephalus, brain abscess, cerebral neoplasm and many others.

Hydrocephalus

Hydrocephalus is a pathological condition that has excess CSF within the ventricular system of the brain, which may or may not increase intracranial pressure. It can be either obstructive or communicating patterns. Communicating hydrocephalus without elevation of CSF pressures can be caused by traumatic injury, prior SAH, and meningitis. Idiopathic normal-pressure hydrocephalus in some patients has the characteristics of the triad of gait apraxia or ataxia, urinary incontinence, and dementia (115-117).

In MRI, hydrocephalus exhibits enlargement of the lateral and third ventricles more than the cortical sulcal enlargement (*Figure 4A*). Moreover, sites of obstructive hydrocephalus can also be identified, such as the fourth ventricle where tumors block the fluid flow (123). A patient-specific 3D geometry of the CSF spaces can be presented in structural MRI. Using phase contrast MRI can measure maximum velocity at the cerebral aqueduct and validate the computational fluid dynamic simulation, thereby highlighting patient-specific boundary conditions. Using volumetric flow-rate boundary conditions can account for deformation of brain tissue through calculation of the conservation of mass. Childhood hydrocephalus commonly has high grade venous stenosis and cerebral hyperemia wherein high grade stenosis can cause conservative management failure while hyperemia is a sign of good prognosis (115,124,125).

Brain abscess

A brain abscess has the feature of a pus-filled swelling caused by bacterial or fungal infection of the brain tissue or severe head injury (126,127). Neuroimaging of a brain abscess relies on the stage of the abscess at imaging and the etiology of the abscess. Brain abscess presents as clear ring-enhancing lesions (*Figure 4B*) (118,128,129) in DWI and perfusion imaging, which is clearly different from necrotic tumors.

Cerebral neoplasm or brain tumors

They are abnormal brain tissue masses resulting from excessive growth of brain cells or a metastatic tumor from other organ systems. Brain tumors can be malignant and grow quickly or benign and grow slowly, and their size and exact position can be identified with MRI optimally (*Figure 4C*). Since primary cerebral neoplasm is uncommon, other parts of the body, such as lungs, colon or breasts, should also be examined to see if the tumor has spread in advanced MRIs, such as diffusion, perfusion, spectroscopy, tractography, and functional MRI. Contrast-enhancing tumor region with high baseline magnetic susceptibility can be reduced markedly by hyperoxic challenges and enforced by hypercapnia relative to hyperoxia. Malignant tumor tissue magnetic susceptibility at baseline under normoxia is correlated with the corresponding susceptibility reduction under hypercapnia. By contrast, necrotic tissue and edema regions do not have dramatic changes in paramagnetic shift (119,130-132).

Others

Many other diseases also show brain lesions and can be specifically diagnosed with MRI, such as sporadic Creutzfeldt-Jakob disease. In MRI, basal ganglia abnormalities and 'cortical ribboning' in the frontal and parietal cortex are typical features of sporadic Creutzfeldt-Jakob disease (*Figure 4D*). Among several types of sporadic Creutzfeldt-Jakob disease, MM2-cortical-type is difficult to be diagnosed on the basis of clinical presentation and laboratory tests. However, MRI has high sensitivity and specificity for it at the early stage by identification of cortical distribution of hyperintensity lesions on DWI in a slower disease progression (120,133).

Demyelinating lesions of multiple sclerosis can cause many cerebral symptoms including ophthalmoplegia (134). In relapsing-remitting multiple sclerosis patients underwent a 7T MRI, relative to the contralateral normal appearing white matter, both enhancing and non-enhancing lesions significantly decrease the amplitude of myelin water but increase interstitial and axonal water (*Figure 4E*). In addition, longer relaxation time is present at interstitial and axonal water, and lower frequency shift appears in axonal water in comparison with the contralateral normal appearing white matter (121,135). Another example is ataxic hemiparesis caused by corticospinal tract impairment. Ataxic hemiparesis possesses typical lacunar syndrome involving

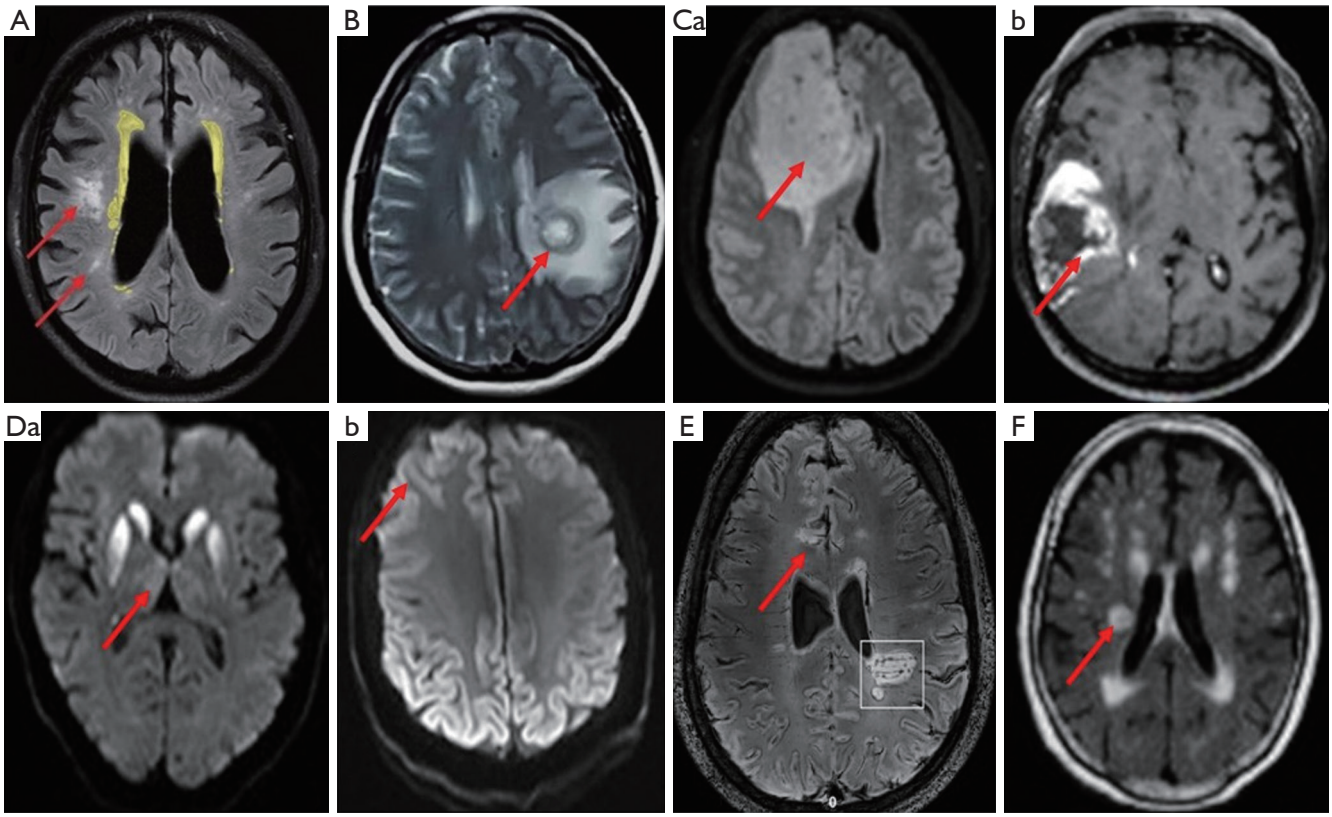

Figure 4 MRI illustration of other brain diseases mimicking CVDs. (A) Hydrocephalus: image showing the periventricular hyperintensities including adjacent changes, but excluding non-adjacent changes in deep white matter. The red arrows mark some of the areas detected as isolated deep white matter changes [reprinted with permission from Snöbohm *et al.* (115)]. (B) Brain abscess. In the left basal ganglia area, an aberrant, circular space-occupying lesion with long T1 and long T2 signal shadows is present. Its ring wall has relatively even thickness, manifesting as slightly short T1 and T2 signal shadows. The lesion-surrounding area contains patches of apparent edema; the left ventricle displays slight compression-resulted deformation; and the midline structures display minor rightward shift [reprinted with permission from Zhou *et al.* (118)]. (C) Brain tumors: representative images of patients with astrocytoma (a) and glioblastoma (b) [reprinted with permission from Sartoretti *et al.* (119)]. (D) Sporadic Creutzfeldt-Jakob disease. DWI shows typical basal ganglia abnormalities (a) and typical features of 'cortical ribboning' in the frontal and parietal cortex (b) [reprinted with permission from Rudge *et al.* (120)]. (E) Multiple sclerosis. 7 T FLAIR-SWI data show several typical white matter hyperintense lesions and global brain atrophy (a) and one large periventricular hyperintense lesion with an encircling hypointense rim (white rectangle, b). Within this lesion, tubular hypointense structures suggestive of veins and circumscribed nodular hypointensities are visible [reprinted with permission from Dal-Bianco *et al.* (121). (F) Ataxic hemispheres. Image exhibits small, round, high, and central low-signal-intensity lesions in the right frontal lobe and internal capsule in T2/FLAIR [reprinted with permission from Lee *et al.* (122)]. Red arrows in B-F point to the typical lesions. MRI, magnetic resonance imaging; CVDs, cerebrovascular diseases; DWI, diffusion-weighted imaging; FLAIR, fluid-attenuated inversion recovery; SWI, susceptibility-weighted imaging.

homolateral ataxia. It often shows central low-signal-intensity lesions in internal capsule in T2/FLAIR image alongside multiple small hyperintensity lesions in both cerebral hemispheres (*Figure 4F*). It can be caused by many different factors including ischemic stroke, mutations in POLR3A characterized by high phenotypic heterogeneity including central hypomyelination in MRI (122,136).

Strengths, limitations and perspectives

Strengths of this review

MRIs do not use radiation that is used by X-rays, CT

scan and PET scans and thus can assess brain function noninvasively. However, MRIs can produce very high resolution, and thus become the imaging technique of choice for diagnosing CVDs. In addition, MRI can be used for treatments as a surgical guidance and assistance in cancer removal (137). For instance, in radiotherapy to treat cancers, MRI-guided linear accelerator can categorize tissues with a high level of spatial and temporal resolution and distinguish malignant from or non-malignant tissues anatomically and functionally while monitoring changes in tissue blood flow. The "real-time" nature of MRI is more suitable for treatment of motile soft-tissue organs, e.g., blood vessel and normal breathing (138-140).

Limitations and contraindications

While MRI represents the frontiers of modern neuroimaging techniques, there are restrictions and contraindications in using MRI techniques due to magnetic fields, machine structure, and gadolinium contrast agents. In general, relative to other neuroimaging techniques, MRIs are more expensive, require the person being scanned to stay completely still for capturing a clear image, take longer for the scan and are not suitable for emergencies like stroke and traumatic injuries. MRIs may also risk the health of specific persons including those who have implants like artificial joints, eye implants, an intrauterine device and a pacemaker. The strong static magnetic field can draw ferromagnetic objects toward MRI scanners of the machine and thus produce projectile effect, twisting, burning, and artifacts. Thus, MRIs may cause displacement of metal implants and device malfunction of foreign bodies, increase body temperature during long MRIs and result in claustrophobia. The loud noises can cause hearing issues. In some MRI scans that need injection of contrast agent, side effects like feeling or being sick may occur.

In the application of MRIs, one major challenge is that MRIs can provide clues of a specific malfunction, but are unable to determine whether abnormal image of tissues are functioning abnormally. As an optimal imaging technique, most MRI sequences are insufficient for diagnosing the functional states. For example, occlusion of a small branch of a cerebral artery may not cause malfunction of the brain region receiving its irrigation because collateral circulation from the Circle of Willis can compensate deficits in blood circulation. Another limitation is that MRIs could not determine functional change involving neurons and non-neuronal cells. Because certain brain areas highlighting on MRIs may represent many functionally diverse neuronal populations, even in one millimeter square area, exact interpretation of brain activity represented by the regional image is difficult. Thus, over-examination with MRIs without specific clinical signs and symptoms may cause confusion rather than clarification of the patient's diseases. Occasionally, false positives or negatives of imaging findings are present in association with functional impairments.

Perspectives of MRI using in diagnosis of CVDs

In order to overcome the limitations potentially associated with the use of MRI in CVDs, it is necessary to have a full understanding of the indications and limitations of MRIs for individual patients. Meanwhile, reducing the expenses, noises, and uncomfortable environment should be the targets of medical industry while standard practice in MRI examination should be followed, such as screening all patients individually for foreign bodies before performing an MRI scan. To remove the labeling of "a high-tech version of phrenology", it is important to combine MRIs with other functional methods, such as combinations of the time resolution of electroencephalogram, source localization in MRI, and multivariate modeling (141). Further detection of changes in regional ionic and neurochemical levels that change accompanying with alterations in local neural activity may provide a more complete and precise picture of brain activity, thereby compensating the insufficiency of neuroimaging techniques.

Conclusions

While stroke and other CVDs can be diagnosed with the support of clear and unique MRI results, differential diagnosis between them with MRI is naturally available in combination with clinical presentation, laboratory tests and other neuroimaging techniques. In MRIs, different CVDs alone or in combination with other primary or secondary cerebral vessel disorders exhibit different hemodynamic, water movement, blood components, myelin, and different association with vessel walls. In ischemic stroke, high DWI/ADC alongside slow or stagnant flow and thromboembolism in vessels are the key MRI signs for early diagnosis with or without other complications. In hemorrhagic stroke, the presence of hematoma and reduced brain volume are the representative neuroimaging. Other CVDs usually have clear signs of cerebral lesions with or without hemodynamic alterations; however, changes in hemodynamic are largely secondary. With the progress of diseases and proceeding of treatments, MRI signs exhibit corresponding changes

that provide further hints for differential diagnosis, understanding the underlying mechanisms, prediction of disease progression and treatment options. Thus, MRI techniques are powerful for differentiating the causes of CVDs, either resulting from cerebral vessel pathogenesis, functional disorders or structural alteration in parenchymal cerebral abnormalities. Fully using the advantages of MRI tests while breaking its limitations is increasingly important for enhancing overall capacity of clinical management of CVDs.

Acknowledgments

We thank Zhengzhou Wenxing Translation Service Co., Ltd. (51scihelp, Certificate No. 298FGY6Y896) for language editing service.
Funding: None.

Footnote

Reporting Checklist: The authors have completed the Narrative Review reporting checklist. Available at https://qims.amegroups.com/article/view/10.21037/qims-22-750/rc

Conflicts of Interest: All authors have completed the ICMJE uniform disclosure form (available at https://qims.amegroups.com/article/view/10.21037/qims-22-750/coif). The authors have no conflicts of interest to declare.

Ethical Statement: The authors are accountable for all aspects of the work in ensuring that questions related to the accuracy or integrity of any part of the work are appropriately investigated and resolved.

References

1. Salmela MB, Mortazavi S, Jagadeesan BD, Broderick DF, Burns J, et al. ACR Appropriateness Criteria(®) Cerebrovascular Disease. J Am Coll Radiol 2017;14:S34-61.
2. Mazzacane F, Mazzoleni V, Scola E, Mancini S, Lombardo I, Busto G, Rognone E, Pichiecchio A, Padovani A, Morotti A, Fainardi E. Vessel Wall Magnetic Resonance Imaging in Cerebrovascular Diseases. Diagnostics (Basel) 2022;12:258.
3. Grosset L, Jouvent E. Cerebral Small-Vessel Diseases: A Look Back from 1991 to Today. Cerebrovasc Dis 2022;51:131-7.
4. Wåhlin A, Eklund A, Malm J. 4D flow MRI hemodynamic biomarkers for cerebrovascular diseases. J Intern Med 2022;291:115-27.
5. Chen L, Zhao N, Xu S. Research progress of imaging technologies for ischemic cerebrovascular diseases. J Int Med Res 2021;49:300060520972601.
6. Dehkharghani S, Andre J. Imaging Approaches to Stroke and Neurovascular Disease. Neurosurgery 2017;80:991.
7. Seiler A, Nöth U, Hok P, Reiländer A, Maiworm M, Baudrexel S, Meuth S, Rosenow F, Steinmetz H, Wagner M, Hattingen E, Deichmann R, Gracien RM. Multiparametric Quantitative MRI in Neurological Diseases. Front Neurol 2021;12:640239.
8. Son JP, Sung JH, Kim DH, Cho YH, Kim SJ, Chung JW, Chang WH, Kim YH, Kim EH, Moon GJ, Bang OY. Brain morphological and connectivity changes on MRI after stem cell therapy in a rat stroke model. PLoS One 2021;16:e0246817.
9. Czap AL, Sheth SA. Overview of Imaging Modalities in Stroke. Neurology 2021;97:S42-51.
10. Little PV, Kraft SE, Chireh A, Damberg P, Holmin S. Oxygen metabolism MRI - A comparison with perfusion imaging in a rat model of MCA branch occlusion and reperfusion. J Cereb Blood Flow Metab 2020;40:2315-27.
11. Jiang D, Lu H. Cerebral oxygen extraction fraction MRI: Techniques and applications. Magn Reson Med 2022;88:575-600.
12. Tsvetanov KA, Henson RNA, Rowe JB. Separating vascular and neuronal effects of age on fMRI BOLD signals. Philos Trans R Soc Lond B Biol Sci 2021;376:20190631.
13. Guo R, Ma C, Li Y, Zhao Y, Wang T, Li Y, El Fakhri G, Liang ZP. High-Resolution Label-Free Molecular Imaging of Brain Tumor. Annu Int Conf IEEE Eng Med Biol Soc 2021;2021:3049-52.
14. Lepping RJ, Montgomery RN, Sharma P, Mahnken JD, Vidoni ED, Choi IY, Sarnak MJ, Brooks WM, Burns JM, Gupta A. Normalization of Cerebral Blood Flow, Neurochemicals, and White Matter Integrity after Kidney Transplantation. J Am Soc Nephrol 2021;32:177-87.

15. Strasser B, Arango NS, Stockmann JP, Gagoski B, Thapa B, Li X, Bogner W, Moser P, Small J, Cahill DP, Batchelor TT, Dietrich J, van der Kouwe A, White J, Adalsteinsson E, Andronesi OC. Improving D-2-hydroxyglutarate MR spectroscopic imaging in mutant isocitrate dehydrogenase glioma patients with multiplexed RF-receive/B(0) -shim array coils at 3 T. NMR Biomed 2022;35:e4621.
16. Thapa B, Mareyam A, Stockmann J, Strasser B, Keil B, Hoecht P, Carp SA, Li X, Wang Z, Chang YV, Dietrich J, Uhlmann E, Cahill DP, Batchelor T, Wald L, Andronesi OC. In Vivo Absolute Metabolite Quantification Using a Multiplexed ERETIC-RX Array Coil for Whole-Brain MR Spectroscopic Imaging. J Magn Reson Imaging 2022;56:121-33.
17. van den Brink H, Doubal FN, Duering M. Advanced MRI in cerebral small vessel disease. Int J Stroke 2023;18:28-35.
18. Khattar N, Triebswetter C, Kiely M, Ferrucci L, Resnick SM, Spencer RG, Bouhrara M. Investigation of the association between cerebral iron content and myelin content in normative aging using quantitative magnetic resonance neuroimaging. Neuroimage 2021;239:118267.
19. Tisdall MD, Ohm DT, Lobrovich R, Das SR, Mizsei G, Prabhakaran K, Ittyerah R, Lim S, McMillan CT, Wolk DA, Gee J, Trojanowski JQ, Lee EB, Detre JA, Yushkevich P, Grossman M, Irwin DJ. Ex vivo MRI and histopathology detect novel iron-rich cortical inflammation in frontotemporal lobar degeneration with tau versus TDP-43 pathology. Neuroimage Clin 2022;33:102913.
20. Canjels LPW, Jansen JFA, Alers RJ, Ghossein-Doha C, van den Kerkhof M, Schiffer VMMM, Mulder E, Gerretsen SC, Aldenkamp AP, Hurks PPM, van de Ven V, Spaanderman MEA, Backes WH. Blood-brain barrier leakage years after pre-eclampsia: dynamic contrast-enhanced 7-Tesla MRI study. Ultrasound Obstet Gynecol 2022;60:541-8.
21. Canjels LPW, Jansen JFA, van den Kerkhof M, Alers RJ, Poser BA, Wiggins CJ, Schiffer VMMM, van de Ven V, Rouhl RPW, Palm WM, van Oostenbrugge RJ, Aldenkamp AP, Ghossein-Doha C, Spaanderman MEA, Backes WH. 7T dynamic contrast-enhanced MRI for the detection of subtle blood-brain barrier leakage. J Neuroimaging 2021;31:902-11.
22. Chen SP, Wang SJ, Wu CH. Author Response: Blood-Brain Barrier Permeability in Patients With Reversible Cerebral Vasoconstriction Syndrome Assessed With Dynamic Contrast-Enhanced MRI. Neurology 2022;98:383.
23. Lin G, Zhuang C, Shen Z, Xiao G, Chen Y, Shen Y, Zong X, Wu R. APT Weighted MRI as an Effective Imaging Protocol to Predict Clinical Outcome After Acute Ischemic Stroke. Front Neurol 2018;9:901.
24. Qiu Y, Bai H, Chen H, Zhao Y, Luo H, Wu Z, Zhang Z. Susceptibility-weighted imaging at high-performance 0.5T magnetic resonance imaging system: Protocol considerations and experimental results. Front Neurosci 2022;16:999240.
25. Churchill NW, Hutchison MG, Graham SJ, Schweizer TA. Cerebrovascular Reactivity After Sport Concussion: From Acute Injury to 1 Year After Medical Clearance. Front Neurol 2020;11:558.
26. Ferlini L, Ligot N, Rana A, Jodaitis L, Sadeghi N, Destrebecq V, Naeije G. Sensitivity and specificity of vessel wall MRI sequences to diagnose central nervous system angiitis. Front Stroke 2022;1:973517.
27. Malm J, Birnefeld J, Zarrinkoob L, Wåhlin A, Eklund A. Hemodynamic Disturbances in Posterior Circulation Stroke: 4D Flow Magnetic Resonance Imaging Added to Computed Tomography Angiography. Front Neurosci 2021;15:656769.
28. Ganzetti M, Wenderoth N, Mantini D. Whole brain myelin mapping using T1- and T2-weighted MR imaging data. Front Hum Neurosci 2014;8:671.
29. Sone D, Maikusa N, Sato N, Kimura Y, Ota M, Matsuda H. Similar and Differing Distributions Between (18)F-FDG-PET and Arterial Spin Labeling Imaging in Temporal Lobe Epilepsy. Front Neurol 2019;10:318.
30. Qureshi AY, Stevens RD. Mapping the Unconscious Brain: Insights From Advanced Neuroimaging. J Clin Neurophysiol 2022;39:12-21.
31. Zhu L, Zhao W, Chen J, Li G, Qu J. Systematic review and meta-analysis of diagnostic test accuracy (DTA) studies: the role of cerebral perfusion imaging in prognosis evaluation of mild cognitive impairment. Ann Palliat Med 2022;11:673-83.
32. Herting MM, Colby JB, Sowell ER, Nagel BJ. White matter connectivity and aerobic fitness in male adolescents. Dev Cogn Neurosci 2014;7:65-75.
33. Li B, Xu D, Zhou J, Wang SC, Cai YX, Li H, Xu HB. Monitoring Bevacizumab-Induced Tumor Vascular Normalization by Intravoxel Incoherent Motion Diffusion-Weighted MRI. J Magn Reson Imaging 2022;56:427-39.
34. Yin Z, Li X, Zhang Y, Tao J, Yang Y, Fang S, Zhang Z, Yuan Y, Liu Y, Wang S. Correlations between DWI, IVIM, and HIF-1α expression based on MRI and pathology in a murine model of rhabdomyosarcoma. Magn Reson Med 2022;88:871-9.

35. Haller S, Haacke EM, Thurnher MM, Barkhof F. Susceptibility-weighted Imaging: Technical Essentials and Clinical Neurologic Applications. Radiology 2021;299:3-26.
36. Yang D, Qin R, Chu L, Xu H, Ni L, Ma J, Shao P, Huang L, Zhang B, Zhang M, Xu Y. Abnormal Cerebrovascular Reactivity and Functional Connectivity Caused by White Matter Hyperintensity Contribute to Cognitive Decline. Front Neurosci 2022;16:807585.
37. Yew B, Jang JY, Dutt S, Li Y, Sible IJ, Gaubert A, Ho JK, Blanken AE, Marshall A, Shao X, Wang DJJ, Nation DA. Cerebrovascular reactivity deficits in cognitively unimpaired older adults: vasodilatory versus vasoconstrictive responses. Neurobiol Aging 2022;113:55-62.
38. Gutierrez J, Khasiyev F, Liu M, DeRosa JT, Tom SE, Rundek T, Cheung K, Wright CB, Sacco RL, Elkind MSV. Determinants and Outcomes of Asymptomatic Intracranial Atherosclerotic Stenosis. J Am Coll Cardiol 2021;78:562-71.
39. Shaikh R, Sohail S. MRA-based evaluation of anatomical variation of circle of Willis in adult Pakistanis. J Pak Med Assoc 2018;68:187-91.
40. Morgan AG, Thrippleton MJ, Wardlaw JM, Marshall I. 4D flow MRI for non-invasive measurement of blood flow in the brain: A systematic review. J Cereb Blood Flow Metab 2021;41:206-18.
41. Tarumi T, Yamabe T, Fukuie M, Zhu DC, Zhang R, Ogoh S, Sugawara J. Brain blood and cerebrospinal fluid flow dynamics during rhythmic handgrip exercise in young healthy men and women. J Physiol 2021;599:1799-813.
42. Zhuang B, Sirajuddin A, Zhao S, Lu M. The role of 4D flow MRI for clinical applications in cardiovascular disease: current status and future perspectives. Quant Imaging Med Surg 2021;11:4193-210.
43. Thangamathesvaran L, Ong SS, Wang J, Lance E, Tekes A, Scott AW. EVALUATION OF MACULAR FLOW VOIDS ON OPTICAL COHERENCE TOMOGRAPHY ANGIOGRAPHY AS POTENTIAL BIOMARKERS FOR SILENT CEREBRAL INFARCTION IN SICKLE CELL DISEASE. Retina 2022;42:340-7.
44. Shahrouki P, Gupta R, Belani P, Chien A, Doshi AH, De Leacy R, Fifi JT, Mocco J, Nael K. Differential Subsampling with Cartesian Ordering-MRA for Classifying Residual Treated Aneurysms. AJNR Am J Neuroradiol 2022;43:887-92.
45. Laustsen M, Andersen M, Xue R, Madsen KH, Hanson LG. Tracking of rigid head motion during MRI using an EEG system. Magn Reson Med 2022;88:986-1001.
46. Muslim AM, Mashohor S, Gawwam GA, Mahmud R, Hanafi MB, Alnuaimi O, Josephine R, Almutairi AD. Brain MRI dataset of multiple sclerosis with consensus manual lesion segmentation and patient meta information. Data Brief 2022;42:108139.
47. Al-Kawaz M, Cho SM, Gottesman RF, Suarez JI, Rivera-Lara L. Impact of Cerebral Autoregulation Monitoring in Cerebrovascular Disease: A Systematic Review. Neurocrit Care 2022;36:1053-70.
48. Badi MK, Vilanilam GK, Gupta V, Barrett KM, Lesser ER, Cochuyt JJ, Hodge DO, Brott TG, Meschia JF. Pharmacotherapy for Patients with Atrial Fibrillation and Cerebral Microbleeds. J Stroke Cerebrovasc Dis 2019;28:2159-67.
49. Elbers J, Armstrong D, Benseler SM, Dlamini N, Steinberg GK, Yeom KW. The Utility of Collaterals as a Biomarker in Pediatric Unilateral Intracranial Arteriopathy. Pediatr Neurol 2018;78:27-34.
50. Frantellizzi V, Pani A, Ricci M, Locuratolo N, Fattapposta F, De Vincentis G. Neuroimaging in Vascular Cognitive Impairment and Dementia: A Systematic Review. J Alzheimers Dis 2020;73:1279-94.
51. Ha SH, Chang JY, Lee SH, Lee KM, Heo SH, Chang DI, Kim BJ. Mechanism of Stroke According to the Severity and Location of Atherosclerotic Middle Cerebral Artery Disease. J Stroke Cerebrovasc Dis 2021;30:105503.
52. Luby M, Merino JG, Davis R, Ansari S, Fisher M, Hsia AW, Kim Y, Latour LL, McCreedy ES, Sukhdeo Singh R, Wright CB, Lynch JK. Association of Multiple Passes during Mechanical Thrombectomy with Incomplete Reperfusion and Lesion Growth. Cerebrovasc Dis 2022;51:394-402.
53. Wu D, Zhou Y, Cho J, Shen N, Li S, Qin Y, Zhang G, Yan S, Xie Y, Zhang S, Zhu W, Wang Y. The Spatiotemporal Evolution of MRI-Derived Oxygen Extraction Fraction and Perfusion in Ischemic Stroke. Front Neurosci 2021;15:716031.
54. Tan MY, Singhal S, Ma H, Chandra RV, Cheong J, Clissold BB, Ly J, Srikanth V, Phan TG. Examining Subcortical Infarcts in the Era of Acute Multimodality CT Imaging. Front Neurol 2016;7:220.
55. Karayiannis C, Soufan C, Chandra RV, Phan TG, Wong K, Singhal S, Slater LA, Ly J, Moran C, Srikanth V. Prevalence of Brain MRI Markers of Hemorrhagic Risk in

Patients with Stroke and Atrial Fibrillation. Front Neurol 2016;7:151.
56. Schlemm L, Braemswig TB, Boutitie F, Vynckier J, Jensen M, Galinovic I, et al. Cerebral Microbleeds and Treatment Effect of Intravenous Thrombolysis in Acute Stroke: An Analysis of the WAKE-UP Randomized Clinical Trial. Neurology 2022;98:e302-14.
57. Choi PK, Chung JY, Lee SJ, Kang HG. Recurrent cerebral microbleeds with acute stroke symptoms: A case report. Medicine (Baltimore) 2018;97:e12480.
58. Ohki A, Saito S, Hata J, Okano HJ, Higuchi T, Fukuchi K. Neurite orientation dispersion and density imaging for evaluating the severity of neonatal hypoxic-ischemic encephalopathy in rats. Magn Reson Imaging 2019;62:214-9.
59. Gómez-Lado N, López-Arias E, Iglesias-Rey R, Díaz-Platas L, Medín-Aguerre S, Fernández-Ferreiro A, Posado-Fernández A, García-Varela L, Rodríguez-Pérez M, Campos F, Del Pino P, Ruibal Á, Pardo-Montero J, Castillo J, Aguiar P, Sobrino T. [18F]-FMISO PET/MRI Imaging Shows Ischemic Tissue around Hematoma in Intracerebral Hemorrhage. Mol Pharm 2020;17:4667-75.
60. Perez FA, Oesch G, Amlie-Lefond CM. MRI Vessel Wall Enhancement and Other Imaging Biomarkers in Pediatric Focal Cerebral Arteriopathy-Inflammatory Subtype. Stroke 2020;51:853-9.
61. Wang GC, Chen YJ, Feng XR, Feng PY. Diagnostic value of HR-MRI and DCE-MRI in unilateral middle cerebral artery inflammatory stenosis. Brain Behav 2020;10:e01732.
62. Danyel LA, Bohner G, Connolly F, Siebert E. Standard Diffusion-weighted MRI for the Diagnosis of Central Retinal Artery Occlusion: A Case-Control Study. Clin Neuroradiol 2021;31:619-26.
63. Zwartbol MH, Rissanen I, Ghaznawi R, de Bresser J, Kuijf HJ, Blom K, Witkamp TD, Koek HL, Biessels GJ, Hendrikse J, Geerlings MI. Cortical cerebral microinfarcts on 7T MRI: Risk factors, neuroimaging correlates and cognitive functioning - The Medea-7T study. J Cereb Blood Flow Metab 2021;41:3127-38.
64. Zhang J, Peng K, Ye F, Koduri S, Hua Y, Keep RF, Xi G. Acute T2*-Weighted Magnetic Resonance Imaging Detectable Cerebral Thrombosis in a Rat Model of Subarachnoid Hemorrhage. Transl Stroke Res 2022;13:188-96.
65. Arts T, Siero JCW, Biessels GJ, Zwanenburg JJM. Automated Assessment of Cerebral Arterial Perforator Function on 7T MRI. J Magn Reson Imaging 2021;53:234-41.
66. Perosa V, Arts T, Assmann A, Mattern H, Speck O, Oltmer J, Heinze HJ, Düzel E, Schreiber S, Zwanenburg JJM. Pulsatility Index in the Basal Ganglia Arteries Increases with Age in Elderly with and without Cerebral Small Vessel Disease. AJNR Am J Neuroradiol 2022;43:540-6.
67. Heit JJ, Iv M, Wintermark M. Imaging of Intracranial Hemorrhage. J Stroke 2017;19:11-27.
68. Abraham PJ, Black JA, Griffin RL, Abraham MN, Liptrap EJ, Thaci B, Holcomb JB, Kerby JD, Harrigan MR, Jansen JO. Imaging analysis of ischemic strokes due to blunt cerebrovascular injury. J Trauma Acute Care Surg 2022;92:990-6.
69. Choi EY, Nieves GA, Jones DE. Acute Stroke Diagnosis. Am Fam Physician 2022;105:616-24.
70. Haque ME, Boren SB, Arevalo OD, Gupta R, George S, Parekh MA, Zhao X, Aronowski J, Savitz SI. Longitudinal, Quantitative, Multimodal MRI Evaluation of Patients With Intracerebral Hemorrhage Over the First Year. Front Neurol 2021;12:764718.
71. Schirmer MD, Dalca AV, Sridharan R, Giese AK, Donahue KL, Nardin MJ, et al. White matter hyperintensity quantification in large-scale clinical acute ischemic stroke cohorts - The MRI-GENIE study. Neuroimage Clin 2019;23:101884.
72. van der Kleij LA, De Vis JB, Restivo MC, Turtzo LC, Hendrikse J, Latour LL. Subarachnoid Hemorrhage and Cerebral Perfusion Are Associated with Brain Volume Decrease in a Cohort of Predominantly Mild Traumatic Brain Injury Patients. J Neurotrauma 2020;37:600-7.
73. Khaladkar SM, Chanabasanavar V, Dhirawani S, Thakker V, Dilip D, Parripati VK. Susceptibility Weighted Imaging: An Effective Auxiliary Sequence That Enhances Insight Into the Imaging of Stroke. Cureus 2022;14:e24918.
74. Yuan J, Jia Z, Song Y, Hu W. External Validation of the Diagnosis of TIA (DOT) Score for Identification of TIA in a Chinese Population. Front Neurol 2019;10:796.
75. Bhat V, Kodapala S. Transient Ischemic Attack Due to Unruptured Basilar Artery Aneurysm. Cureus 2022;14:e24102.
76. Zhou J, He R, Xu X, Wei X, Li M, Wang F, Li Y. Diffusion kurtosis imaging in patients with tissue-negative transient ischemic attack. Front Neurol 2022;13:1052310.
77. Zhang F, Xue Y, Zhang F, Wei X, Zhou Z, Ma Z, Wang X, Shen H, Li Y, Cui X, Liu L. Identification of a Novel CCM1 Frameshift Mutation in a Chinese Han Family With Multiple Cerebral Cavernous Malformations. Front

Neurosci 2020;14:525986.
78. Park MS, Kwon S, Lee MJ, Kim KH, Jeon P, Park YJ, Kim DI, Kim YW, Bang OY, Chung CS, Lee KH, Kim GM. Identification of High Risk Carotid Artery Stenosis: A Multimodal Vascular and Perfusion Imaging Study. Front Neurol 2019;10:765.
79. Sollmann N, Liebl H, Preibisch C, Zimmer C, Helle M, Obara M, Kirschke JS, Kaczmarz S. Super-selective ASL and 4D ASL-based MR Angiography in a Patient with Moyamoya Disease: Case Report. Clin Neuroradiol 2021;31:515-9.
80. Kopczak A, Schindler A, Sepp D, Bayer-Karpinska A, Malik R, Koch ML, Zeller J, Strecker C, Janowitz D, Wollenweber FA, Hempel JM, Boeckh-Behrens T, Cyran CC, Helck A, Harloff A, Ziemann U, Poli S, Poppert H, Saam T, Dichgans M. Complicated Carotid Artery Plaques and Risk of Recurrent Ischemic Stroke or TIA. J Am Coll Cardiol 2022;79:2189-99.
81. Shima H, Taguchi H, Niwa Y, Bandoh K, Watanabe Y, Yamashita K, Shimazaki K, Koyasu H, Hasegawa Y; . Stroke Risk in Patients with Suspected Transient Ischemic Attacks with Focal and Nonfocal Symptoms: A Prospective Study. J Stroke Cerebrovasc Dis 2022;31:106185.
82. Schmitzer L, Sollmann N, Kufer J, Kallmayer M, Eckstein HH, Zimmer C, Preibisch C, Kaczmarz S, Göttler J. Decreasing Spatial Variability of Individual Watershed Areas by Revascularization Therapy in Patients With High-Grade Carotid Artery Stenosis. J Magn Reson Imaging 2021;54:1878-89.
83. Deguchi K, Kawahara Y, Deguchi S, Morimoto N, Kurata T, Ikeda Y, Ichikawa T, Tokunaga K, Kawai N, Sugiu K, Abe K. A patient develops transient unique cerebral and cerebellar lesions after unruptured aneurysm coiling. BMC Neurol 2015;15:49.
84. Li Y, Kim J, Simpson D, Aagaard-Kienitz B, Niemann D, Esene IN, Ahmed A. Difference in imaging biomarkers between transient and permanent neurological deficits after endovascular treatment of cerebrovascular aneurysms. J Neurosurg 2020;134:1861-70.
85. Zhang J, Brindise MC, Rothenberger SM, Markl M, Rayz VL, Vlachos PP. A multi-modality approach for enhancing 4D flow magnetic resonance imaging via sparse representation. J R Soc Interface 2022;19:20210751.
86. Sindeev S, Arnold PG, Frolov S, Prothmann S, Liepsch D, Balasso A, Berg P, Kaczmarz S, Kirschke JS. Phase-contrast MRI versus numerical simulation to quantify hemodynamical changes in cerebral aneurysms after flow diverter treatment. PLoS One 2018;13:e0190696.
87. Misaki K, Futami K, Uno T, Nambu I, Yoshikawa A, Kamide T, Nakada M. Inflow Hemodynamics of Intracranial Aneurysms: A Comparison of Computational Fluid Dynamics and 4D Flow Magnetic Resonance Imaging. J Stroke Cerebrovasc Dis 2021;30:105685.
88. Al-Mousa A, Altarawneh M, Alqatawneh O, Bashir Z, Al-Dwairy S, Shtaya A. Eosinophilic Granuloma of the Skull Presenting as Non-Traumatic Extradural Haematoma in Children. Int J Gen Med 2020;13:1229-34.
89. Martín-Noguerol T, Concepción-Aramendia L, Lim CT, Santos-Armentia E, Cabrera-Zubizarreta A, Luna A. Conventional and advanced MRI evaluation of brain vascular malformations. J Neuroimaging 2021;31:428-45.
90. da Silva AJF, de Carvalho Ruela Pires AC, de Farias LCL, da Silva CRV. Cerebrofacial vascular metameric syndrome associated with Moyamoya syndrome: a rare case report. Childs Nerv Syst 2022;38:801-5.
91. Clark M, Unnam S, Ghosh S. A review of carotid and vertebral artery dissection. Br J Hosp Med (Lond) 2022;83:1-11.
92. Cirillo L, Rustici A, Toni F, Zoli M, Bartiromo F, Gramegna LL, Cicala D, Tonon C, Caranci F, Lodi R. Vessel Wall MRI: clinical implementation in cerebrovascular disorders-technical aspects. Radiol Med 2022;127:645-51.
93. Wang X, Qiao T, Liu M, Wang X. Homocysteine Associated With Low Cognitive Function Independent of Asymptomatic Intracranial and Carotid Arteries Stenoses in Chinese Elderly Patients: An Outpatient-Based Cross-Sectional Study. J Geriatr Psychiatry Neurol 2022;35:302-8.
94. Weiner S, Benton MH, Guraziu B, Yange Y, He J, Chen YT, Marston WA, McGinigle KL. High Stroke Rate in Patients With Medically Managed Asymptomatic Carotid Stenosis at an Academic Center in the Southeastern United States. Ann Vasc Surg 2022;85:418-23.
95. Zhang J, Yan Y, Yao W, Liu J, Cui L. Multimodality imaging of carotid web: A case report and literature review. Vascular 2022. [Epub ahead of print]. doi: 10.1177/17085381221084809.
96. Nam KW, Kwon HM, Jeong HY, Park JH, Kwon H, Jeong SM. Intracranial Atherosclerosis and Stage 1 Hypertension Defined by the 2017 ACC/AHA Guideline. Am J Hypertens 2020;33:92-8.
97. Liu P, Liu G, Pinho MC, Lin Z, Thomas BP, Rundle M, Park DC, Huang J, Welch BG, Lu H. Cerebrovascular

Reactivity Mapping Using Resting-State BOLD Functional MRI in Healthy Adults and Patients with Moyamoya Disease. Radiology 2021;299:419-25.
98. Yamashita K, Sugimori H, Nakamizo A, Amano T, Kuwashiro T, Watanabe T, Kawamata K, Furuya K, Harada S, Kamei R, Maehara J, Okada Y, Noguchi T. Different hemodynamics of basal ganglia between moyamoya and non-moyamoya diseases using intravoxel incoherent motion imaging and single-photon emission computed tomography. Acta Radiol 2022. [Epub ahead of print]. doi: 10.1177/02841851221092895.
99. Nishizawa T, Fujimura M, Katsuki M, Mugikura S, Tashiro R, Sato K, Tominaga T. Prediction of Cerebral Hyperperfusion after Superficial Temporal Artery-Middle Cerebral Artery Anastomosis by Three-Dimensional-Time-of-Flight Magnetic Resonance Angiography in Adult Patients with Moyamoya Disease. Cerebrovasc Dis 2020;49:396-403.
100. Dobashi K, Kubo Y, Kimura K, Katakura Y, Chida K, Kobayashi M, Yoshida K, Fujiwara S, Terasaki K, Ogasawara K. De Novo Cerebral Microbleeds and Cognitive Decline in Cerebral Hyperperfusion After Direct Revascularization for Adult Moyamoya Disease. J Stroke Cerebrovasc Dis 2022;31:106166.
101. Katakura Y, Kubo Y, Dobashi K, Kimura K, Fujiwara S, Chida K, Kobayashi M, Yoshida K, Terasaki K, Ogasawara K. Delayed development of cerebral atrophy after cerebral hyperperfusion following arterial bypass for adult patients with ischemic moyamoya disease: supplementary analysis of a 5-year prospective cohort. Acta Neurochir (Wien) 2022;164:1037-45.
102. Ren S, Wu W, Su C, Zhu Q, Schmidt M, Sun Y, Forman C, Speier P, Hong X, Lu S. High-resolution compressed sensing time-of-flight MR angiography outperforms CT angiography for evaluating patients with Moyamoya disease after surgical revascularization. BMC Med Imaging 2022;22:64.
103. Zerweck L, Roder C, Hauser TK, Thurow J, Mengel A, Tatagiba M, Khan N, Meyer PT, Ernemann U, Klose U. Hemodynamic evaluation of patients with Moyamoya Angiopathy: comparison of resting-state fMRI to breath-hold fMRI and [15O]water PET. Neuroradiology 2022;64:553-63.
104. Yamashita C, Shigeto H, Maeda N, Kawaguchi M, Uryu M, Motomura S, Kira J. Transient interhemispheric disconnection in a case of insulinoma-induced hypoglycemic encephalopathy. J Neurol Sci 2013;335:233-7.
105. Ren S, Chen Z, Liu M, Wang Z. The radiological findings of hypoglycemic encephalopathy: A case report with high b value DWI analysis. Medicine (Baltimore) 2017;96:e8425.
106. Akinseye L, Ward J, Lahoti A. Hemiparesis With Hypoglycemia in a Child With Hypopituitarism Involving LHX4 Gene Deletion. Pediatrics 2022;149:e2021050995.
107. Zhang W, Wang S, Wang C, Liu L, Lin P, Li F, Wu L, Zou R. Head-up tilt test results in child twins with nervous mediated syncope. Int J Cardiol 2016;221:194-7.
108. El Nahas NM, Aref HM, Alloush TK, Fahmy NA, Ahmed KA, El Basiouny AA, Tork MA, Elbokl AM, Shokri HM. Borderzone Infarction and Small Vessel Disease in a Sample of Egyptian Stroke Patients: Differences and Similarities. Neurol India 2021;69:670-5.
109. Longarzo M, Cavaliere C, Mele G, Tozza S, Tramontano L, Alfano V, Aiello M, Salvatore M, Grossi D. Microstructural Changes in Motor Functional Conversion Disorder: Multimodal Imaging Approach on a Case. Brain Sci 2020.
110. Perez DL, LaFrance WC Jr. Nonepileptic seizures: an updated review. CNS Spectr 2016;21:239-46.
111. Feinstein A, Voon V. Understanding conversion disorder: How contemporary brain imaging is shedding light on an early Freudian concept. J Psychiatr Res 2021;141:353-7.
112. Suwanwela NC, Kijpaisalratana N, Tepmongkol S, Rattanawong W, Vorasayan P, Charnnarong C, Tantivattana J, Roongruang S, Ongphichetmetha T, Panjasriprakarn P, Chutinet A, Akarathanawat W, Saver JL. Prolonged migraine aura resembling ischemic stroke following CoronaVac vaccination: an extended case series. J Headache Pain 2022;23:13.
113. Antonucci MU, Yazdani M. A Helpful Tool in Diagnosing Stroke Mimics: Arterial Spin Labeled Perfusion Magnetic Resonance Imaging. J Emerg Med 2020;58:439-43.
114. Jurkiewicz MT, Vossough A, Pollock AN. An Important Pediatric Stroke Mimic: Hemiplegic Migraine. Can J Neurol Sci 2020;47:235-6.
115. Snöbohm C, Malmberg F, Freyhult E, Kultima K, Fällmar D, Virhammar J. White matter changes should not exclude patients with idiopathic normal pressure hydrocephalus from shunt surgery. Fluids Barriers CNS 2022;19:35.
116. Tseng PH, Wu LK, Wang YC, Ho TJ, Lin SZ, Tsai ST. Diagnosis and treatment for normal pressure hydrocephalus: From biomarkers identification to outcome improvement with combination therapy. Tzu Chi Med J 2021;34:35-43.

117. Sun Y, Liang S, Yu Y, Yang Y, Lu J, Wu J, Cheng Y, Wang Y, Wu J, Han J, Yu N. Plantar pressure-based temporal analysis of gait disturbance in idiopathic normal pressure hydrocephalus: Indications from a pilot longitudinal study. Comput Methods Programs Biomed 2022;217:106691.
118. Zhou W, Shao X, Jiang X. A Clinical Report of Two Cases of Cryptogenic Brain Abscess and a Relevant Literature Review. Front Neurosci 2019;12:1054.
119. Sartoretti E, Sartoretti T, Wyss M, Reischauer C, van Smoorenburg L, Binkert CA, Sartoretti-Schefer S, Mannil M. Amide proton transfer weighted (APTw) imaging based radiomics allows for the differentiation of gliomas from metastases. Sci Rep 2021;11:5506.
120. Rudge P, Hyare H, Green A, Collinge J, Mead S. Imaging and CSF analyses effectively distinguish CJD from its mimics. J Neurol Neurosurg Psychiatry 2018;89:461-6.
121. Dal-Bianco A, Grabner G, Kronnerwetter C, Weber M, Höftberger R, Berger T, Auff E, Leutmezer F, Trattnig S, Lassmann H, Bagnato F, Hametner S. Slow expansion of multiple sclerosis iron rim lesions: pathology and 7 T magnetic resonance imaging. Acta Neuropathol 2017;133:25-42.
122. Lee JH, Heo SH, Lee JS, Chang DI, Park KH, Sung JY, Hong IK, Kim MH, Park BJ, Choi WS. Acute Hemiparesis in a Healthy Elderly Woman: Where and What Is the Lesion? Front Neurol 2017;8:109.
123. Toescu SM, Samarth G, Layard Horsfall H, Issitt R, Margetts B, Phipps KP, Jeelani NU, Thompson DNP, Aquilina K. Fourth ventricle tumors in children: complications and influence of surgical approach. J Neurosurg Pediatr 2020;27:52-61.
124. Bateman GA, Yap SL, Subramanian GM, Bateman AR. The incidence of significant venous sinus stenosis and cerebral hyperemia in childhood hydrocephalus: prognostic value with regards to differentiating active from compensated disease. Fluids Barriers CNS 2020;17:33.
125. Griffa A, Van De Ville D, Herrmann FR, Allali G. Neural circuits of idiopathic Normal Pressure Hydrocephalus: A perspective review of brain connectivity and symptoms meta-analysis. Neurosci Biobehav Rev 2020;112:452-71.
126. Ma Y, Li W, Ao R, Lan X, Li Y, Zhang J, Yu S. Central nervous system aspergillosis in immunocompetent patients: Case series and literature review. Medicine (Baltimore) 2020;99:e22911.
127. Yoon EJ, Jasinski JM, Tong D, Kado K, Richards B, Mccabe RW. Encapsulated Intracerebral Hematoma Presenting as Cerebral Abscess. Cureus 2021;13:e15198.
128. Ozbayrak M, Ulus OS, Berkman MZ, Kocagoz S, Karaarslan E. Atypical pyogenic brain abscess evaluation by diffusion-weighted imaging: diagnosis with multimodality MR imaging. Jpn J Radiol 2015;33:668-71.
129. Ganau M, Mankad K, Srirambhatla UR, Tahir Z, D'Arco F. Ring-enhancing lesions in neonatal meningitis: an analysis of neuroradiology pitfalls through exemplificative cases and a review of the literature. Quant Imaging Med Surg 2018;8:333-41.
130. Sanders JW, Chen HS, Johnson JM, Schomer DF, Jimenez JE, Ma J, Liu HL. Synthetic generation of DSC-MRI-derived relative CBV maps from DCE MRI of brain tumors. Magn Reson Med 2021;85:469-79.
131. Stokes AM, Bergamino M, Alhilali L, Hu LS, Karis JP, Baxter LC, Bell LC, Quarles CC. Evaluation of single bolus, dual-echo dynamic susceptibility contrast MRI protocols in brain tumor patients. J Cereb Blood Flow Metab 2021;41:3378-90.
132. Scola E, Desideri I, Bianchi A, Gadda D, Busto G, Fiorenza A, Amadori T, Mancini S, Miele V, Fainardi E. Assessment of brain tumors by magnetic resonance dynamic susceptibility contrast perfusion-weighted imaging and computed tomography perfusion: a comparison study. Radiol Med 2022;127:664-72.
133. Hamaguchi T, Sanjo N, Ae R, Nakamura Y, Sakai K, Takao M, Murayama S, Iwasaki Y, Satoh K, Murai H, Harada M, Tsukamoto T, Mizusawa H, Yamada M. MM2-type sporadic Creutzfeldt-Jakob disease: new diagnostic criteria for MM2-cortical type. J Neurol Neurosurg Psychiatry 2020;91:1158-65.
134. Saeed H, Jawed Q, Noori MAM, Bin Waqar SH, Rehan A. An Unusual Case of Isolated Acute Aphasia in Multiple Sclerosis. Cureus 2021;13:e18278.
135. Li X, van Gelderen P, Sati P, de Zwart JA, Reich DS, Duyn JH. Detection of demyelination in multiple sclerosis by analysis of Formula: see text relaxation at 7 T. Neuroimage Clin 2015;7:709-14.
136. Yamamoto R, Johkura K, Nakae Y, Tanaka F. The mechanism of ipsilateral ataxia in lacunar hemiparesis: SPECT perfusion imaging. Eur Neurol 2015;73:106-11.
137. Stadlbauer A, Merkel A, Zimmermann M, Sommer B, Buchfelder M, Meyer-Bäse A, Rössler K. Intraoperative Magnetic Resonance Imaging of Cerebral Oxygen Metabolism During Resection of Brain Lesions. World Neurosurg 2017;100:388-94.
138. Bruijnen T, van der Heide O, Intven MPW, Mook S, Lagendijk JJW, van den Berg CAT, Tijssen RHN.

Technical feasibility of magnetic resonance fingerprinting on a 1.5T MRI-linac. Phys Med Biol 2020;65:22NT01.
139. Graham JA, Redler G, Delozier KB, Yu HM, Oliver DE, Rosenberg SA. Dosimetric feasibility of hippocampal avoidance whole brain radiotherapy with an MRI-guided linear accelerator. J Appl Clin Med Phys 2022;23:e13587.
140. Shan S, Li M, Li M, Tang F, Crozier S, Liu F. ReUINet: A fast GNL distortion correction approach on a 1.0 T MRI-Linac scanner. Med Phys 2021;48:2991-3002.
141. Ladwig Z, Yu Y, Gratton C. Combined methods reveal task activation dynamics in human brain networks. PLoS Biol 2022;20:e3001749.

Cite this article as: Li X, Su F, Yuan Q, Chen Y, Liu CY, Fan Y. Advances in differential diagnosis of cerebrovascular diseases in magnetic resonance imaging: a narrative review. Quant Imaging Med Surg 2023;13(4):2712-2734. doi: 10.21037/qims-22-750

